sustainability

MDPI

Article

Probability Assessment of the Seismic Risk of Highway Bridges with Various Structural Systems (Case Study: Tehran City)

Meisam Mogheisi [1], Hamidreza Tavakoli [1,*] and Elnaz Peyghaleh [2]

[1] Faculty of Civil Engineering, Babol Noshirvani University of Technology, Babol 47148-71167, Iran; mogheisi@gmail.com
[2] Department of Civil Engineering, Clemson University, Clemson, SC 29634, USA; epeygha@clemson.edu
* Correspondence: tavakoli@nit.ac.ir

Abstract: Considering the development of urban transportation systems and the importance of highway bridges in a city's resilience against earthquakes, it is critical to pay special attention to the seismic risk evaluation of highway bridges. The most significant issue to consider is the assessment of possible direct and indirect damages imposed on bridges before an earthquake. After this, the best practices for bridge rehabilitation can be adopted to minimize the induced damage. In this paper, we assessed the seismic risks associated with all 713 highway bridges in Tehran province (the capital of Iran). These bridges were initially divided into six categories according to their structural system and construction year and were also classified by whether or not seismic design was included. Among the 84,000 earthquakes recommended by the researchers' ten-thousand-year catalog, a set of 50 ground motion records was selected in the course of a probabilistic approach via the Optimization-based Probabilistic Scenarios (OPS) algorithm in an attempt to obtain the least amount of error compared to the original catalog in the final hazard curve in different regions of Tehran province. Afterward, the seismic fragility curves were plotted in four damage states of slight, moderate, extensive, and complete for the six bridge structural systems of simple, steel, concrete slab box, concrete slab–steel box, concrete slab, and steel girder–concrete slab. The results of the fragility curves extracted from the decision tree analysis were validated with those developed from incremental dynamic analysis (IDA) for a bridge case study modeled in the OpenSEES software V2.5.0. Later, using logical relationships, seismic risk curves were drawn for each structural system. The results show that, in general, the average seismic damage of bridges over ten years old is 0.88 times the average damage of bridges less than ten years old. The highest level of vulnerability is associated with the simple bridge system with a median vulnerability of 0.44. Moreover, the lowest level of vulnerability is related to the steel girder–concrete slab bridge system with a median vulnerability of 0.98, showing an increase of approximately 2.2 times in the median vulnerability. In addition, based on the sensitivity analysis results, the indirect and total risk levels increase almost exponentially with increasing the reconstruction index.

Keywords: seismic risk assessment; bridge; fragility curves; reconstruction index

Citation: Mogheisi, M.; Tavakoli, H.; Peyghaleh, E. Probability Assessment of the Seismic Risk of Highway Bridges with Various Structural Systems (Case Study: Tehran City). *Sustainability* **2023**, *15*, 9783. https://doi.org/10.3390/su15129783

Academic Editor: Junsheng Su

Received: 30 March 2023
Revised: 8 June 2023
Accepted: 15 June 2023
Published: 19 June 2023

1. Introduction

Damage imposed on bridges in past earthquakes, which is indicative of a bridge's insufficient seismic performance, not only affects the public transportation system but also disturbs urban and economic activities. Bridge seismic performance depends on factors including geometric characteristics, year of construction, type of structural system, earthquake record specifications, etc.

Before 1971, most bridges were built without considering seismic design requirements. The bridge damage accounts from past earthquakes indicate that the loss to bridge components varies from small cracks in the concrete cover to column failure and collapse of the entire deck. In light of this, different types and degrees of damage to bridge components require different repair methods based on damage type. Therefore, it is crucial to classify

and diagnose the types of bridge failures during earthquakes, as well as to identify the causes and consequences of such failures. Fragility curves are among the most distinguished seismic vulnerability assessment methods widely used in seismic vulnerability investigations in recent years. A fragility curve is considered a key element in the failure analysis examination of structures subjected to earthquakes. It establishes the relationship between the two components of earthquake risk and structural properties [1].

Another dispute, which is of substantial significance, is related to bridge maintenance management. Adopting the most appropriate measure in the maintenance and repair management of bridges, and achieving such a measure that includes factors such as importance, current status and load-bearing capacity of the structure, quality of bridge serviceability, life cycle costs of structure, variations in the future costs in terms of inflation and deflation rates, economic, social, and safety consequences of repair, bridge deterioration, time-dependent degradation rate, and many other factors can be very expensive and complicated. Therefore, the question is: are these measures economical? In fact, the bridge management system is a solution to optimize and manage available resources for inspection, maintenance, or even replacement of bridges. This allows city managers to save hundreds of billions in the repair and maintenance phase through careful planning and avoiding reactive maintenance policies.

From the standpoint of crisis management and seismic risk mitigation, bridge management can be defined as a strategy to get the most positive impact (highest risk mitigation) at the lowest cost. In other words, it addresses the question of how to achieve the highest earthquake risk reduction in bridges at the scale of a metropolis. This is done by spending a certain amount of the annual budget. Moreover, it deals with the process to plan and prioritize retrofitting or rehabilitation of bridges to achieve the highest positive impact on the seismic risk state. This issue has been tackled in the present research by using genetic and branch-and-bound optimization algorithms by examining different scenarios and considering synthetic earthquake catalogs representing long-term seismicity and attenuation functions used to model probabilistic strong ground motions impacting bridges. Each earthquake scenario results in probabilistic and spatial distributions of bridge damages in Tehran province. Furthermore, essential parameters in the optimization procedure have been explored.

Numerous research studies have been carried out to determine the fragility relationships and evaluate the associated risk using simulations via analytical models. In this regard, Ramanathan (2012) conducted a probabilistic seismic damage analysis of bridges in California. Accordingly, 5314 existing bridges in California were classified into 13 different inventories based on their structural system. The frequency of each was calculated. In addition, parameters such as median, standard deviation, and geometric properties were estimated. The fragility curves of each component, as well as the overall bridge system, were plotted in four damage states: slight, moderate, extensive, and complete [2].

Mosleh (2016) investigated the fragility curves of concrete bridges built before 1990 in Iran. Bridge fragility curves were compared in two near-fault and far-field states with three-dimensional (3-D) modeling and non-linear dynamic analysis subjected to 70 earthquake records [3].

Xiang et al. (2019) evaluated the seismic vulnerability of two- and multi-column bridges in near- and far-fault zones. In their study, bridge columns were retrofitted by using either of the three techniques of buckling-restrained braces (BRBs), viscous damper braces (VDBs), or piston-based self-centering braces (PBSCs) [4].

Chen et al. (2020) examined the vulnerability of bridges with tall piers subjected to near-fault excitations in southwest China. The fragility curves for bridges with different heights from 10 to 50 m were then compared. Accordingly, Sa was considered as the earthquake intensity measure to produce fragility curves. The results indicated that bridges with 50-m piers were extremely vulnerable to near-fault excitations [5].

Naseri et al. (2022) performed a probabilistic seismic vulnerability assessment of existing reinforced concrete (RC) curved box-girder bridges with radii of 66, 132, 265, and

1324 m. The investigated bridges were subjected to 80 near-field earthquake records in the OpenSEES software to carry out non-linear dynamic analyses in the two cases of retrofitting with carbon fiber-reinforced polymer (CFRP) and without retrofitting. The fragility curves were then plotted for different components of the bridges by involving 14 sources of uncertainty in the modeling process. The fragility curve of the entire bridge system was then calculated by considering the components in series. The results suggested that the probability of damage extent increased markedly with the reduction of the bridge radius. Additionally, median fragility increased by 32%, on average, after CFRP strengthening. This is indicative of a significant reduction in the bridge's seismic damage level [6].

According to previous studies, researchers have recommended different relationships for the estimation of the risk function, the most prominent of which are briefly mentioned in the following.

Edwards, P.J and Bowen, P.A (1998) presented a risk-taking relationship, expressing that the level of risk-taking is directly related to vulnerability but inversely connected to the level of preparedness. In other words, risk was considered constant and risk-taking variable [7].

In the risk triangle theory proposed by Birkmann (2013), vulnerability was defined as one of the three dimensions in measuring risk tolerance in societies, as regards local crises. However, it was believed that the influential factors in the safekeeping of societies include not only the possibility and intensity of vulnerability, but also the risk-exposed phenomena in relation to the level of sensitivity and capability of society to recover and manage along with possible hazards from other dimensions of measuring risk tolerance [8].

In a different study, Fedeski et al. (2007) introduced a linear relationship for the risk function. In that model, risk-taking was proposed based on the level of vulnerability, hazard, and element exposure to risk [9].

Tsai et al. (2010), while implementing a practical mechanism to assess and manage the risk of 90 earthquake disasters, defined the risk function as the product of three parameters of hazard, exposure, and vulnerability [10].

Masuya (2014) introduced a risk function as the result of risk multiplied by vulnerability while considering the level of preparedness (capacity to deal with risks) of society as part of vulnerability [11].

Si-Qi Li investigated the seismic vulnerability of reinforced concrete girder bridges and reinforced concrete buildings by combining nonlinear vulnerability numerical analysis and probabilistic model analysis. By considering age factors, seismic design, combination of age and seismic design and foundation type factors and using the average damage matrix, he developed the model matrix index calculation and compared the average damage index vulnerability parameters curve of reinforced concrete girder bridges and reinforced concrete buildings in multiple severity areas. In this method, 1069 reinforced concrete girder bridges and 949 reinforced concrete buildings damaged in the Wenchuan earthquake on 12 May 2008 were analyzed, and the grade of vulnerability of the damaged samples was selected based on the China Seismic Intensity Scale (CSIS-08). The vulnerability matrix of reinforced concrete girder bridges and reinforced concrete buildings in multiple-intensity areas was developed by comparing the vulnerability of the curve and taking into account the failure ratio and excess probability and the considered factors [12].

Although many studies have been conducted on the failure probability and the development of fragility curves in structures, particularly bridges, no extensive research has, to date, been carried out on the classification, vulnerability evaluation, and risk level identification of bridges in Tehran province. The main objective of this research is to address this issue.

2. Introducing the Investigated Models

According to an extensive research and data collection, Tehran province, as Iran's capital, has 713 existing highway bridges. Based on the type of structural system, these bridges were classified into six general inventories, as reported in Table 1. Each structural

system was also divided into two categories, with and without seismic design, based on their time of construction.

Table 1. Types of investigated structures for extracting fragility relationships.

Concrete Slab Box (SBCD)	w/seismic design w/o seismic design
Concrete Slab (CD)	w/seismic design w/o seismic design
Concrete Slab–Steel Box (SSCD)	w/seismic design w/o seismic design
Concrete Slab–Steel Girder (CS)	w/seismic design w/o seismic design
Steel (S)	w/seismic design w/o seismic design
Simple (SIM)	w/seismic design w/o seismic design

In order for the probabilistic assessment of the damage level, nine important parameters required for these bridges were collected, as given in Table 2.

Table 2. Database parameters of the existing bridges.

Name in Brief	Description
Build_Year	Year in which the bridge was built
Name	Name of the bridge
Span_NO	Number of spans
Material	Materials used in the bridge
Deck_Type	Type of bridge deck
First_Addr	Bridge location
Local_Name	The local name of the bridge
Shape_Length	The total length of the bridge
Shape_Area	The total area of the bridge

3. Determining the Geographical Coordinates of Bridges

Owing to the large number of bridges, it is not possible to manually determine the spatial coordinates of the bridges correctly and without error. Therefore, the Google Maps API was used to solve this problem. Using the GeoCoding and Inverse GeoCoding features in this API, the bridge location can be obtained from the geographical coordinates. In addition, the geographical coordinates can be attained from the bridge location, respectively. Given that the address field is complete for all bridges within the databank, the geographical coordinates of all bridges were determined through the Inverse Geocoding feature. The distribution of these bridges across Tehran province is shown in Figure 1.

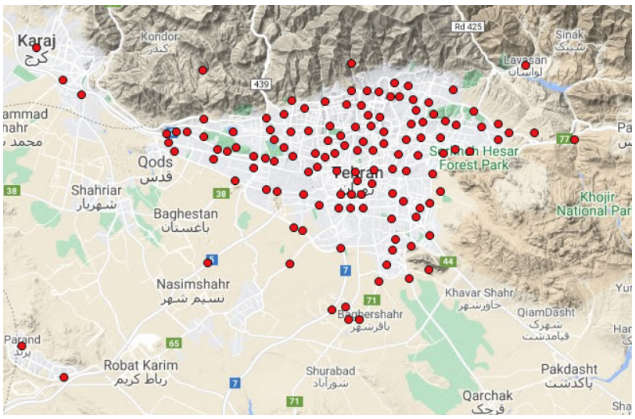

Figure 1. Distribution of highway bridges across Tehran province.

4. Determining the Type of Seismic Design

According to past earthquake experiences, seismic design regulations are constantly changing and improving. In the meantime, significant changes occurred in the design regulations for Iranian bridges in 2001. Therefore, bridges were classified on the basis of whether they followed the seismic design codes or did not include seismic design, based on the construction date of the bridge, available in the databank. In this respect, structures built before 2001 were listed in the "without seismic design" category. Those built after 2001 were categorized as belonging to the "with seismic design" group.

5. Calculating the Financial Value of Bridges

Several vital parameters are involved in the calculation of structure risk, including asset value. This parameter represents how much should be spent to build a bridge similar to an existing one and takes existing defects and shortcomings into account. This amount of cost is considered the current value of the bridge at present. Due to the lack of information on the details of all bridges, approximate relations were used in this research to estimate the value of bridges, as expressed in Equation (1).

$$Value = A \times B \times C \times L \quad (1)$$

In this relation, A is the unit length of a concrete bridge. This was considered equal to 2000 million units in this project. It should be noted that coefficient A can only be applied to concrete bridges. Coefficient B is used for other bridge structural systems. This is the ratio of the unit length value of other structural bridge systems to that of the concrete bridge system. Therefore, coefficient B is related to the type of structural system, whose calculated measures in this research are given in Table 3. Additionally, L represents the bridge's total length.

Table 3. Values of coefficient B for calculating the unit length value of different bridge structural systems.

Type of Bridge Structure	Coefficient B
Simple	0.50
Steel	1.20
Concrete Slab–Steel Girder	1.15
Concrete Slab–Steel Box	1.30
Concrete Slab	1.00
Concrete Slab Box	1.15

Coefficient C denotes the structure's life. Obviously, the older the bridge structure is, the less financial value it has. However, the amount of financial loss will be less in the event of earthquake damage. In order to apply this parameter, the structures were divided into two classes, old and new. The values of coefficient C for each class were proposed according to Table 4.

Table 4. Values of coefficient C according to the age of bridge structure.

Bridge Age	Coefficient C
Equal or less than 10 years	1
More than 10 years	0.9

In spite of this, it should be noted that the proposed relationships and coefficients were derived from an engineering perspective. Nevertheless, one can use the real value of an existing bridge in modeling if it is available.

6. Determining Indirect Damage Ratio (IDR)

Depending on the type of damage, structural damage can be divided into two parts. The direct damage part can be calculated using empirical relationships based on structural damage extent. Indirect damage is determined by a wide variety of factors. For example, when a bridge is out of service, various consequences, such as increased traffic in other roadways, increased fuel consumption, difficulty of access to certain locations, and similar issues, can be conceived of. All these issues, in addition to the direct damage imposed on the bridge structure under the effect of the earthquake, give rise to other damages defined as secondary or indirect damages.

In this research, Equation (2) was used to estimate the IDR caused by highway bridge damage, which itself stems from the direct damage caused by the earthquake.

$$Indirect\ Damage = R \times Direct\ Damage \quad (2)$$

- In this equation, the coefficient R is calculated according to Equation (3), based on two main indices. These two indices are:
- Reconstruction time index (P): Reconstruction time is the time required to rebuild the damaged bridge and restore it to its operation cycle. Such a measure is a function of the capability to cover reconstruction costs. It also includes the time required for removing debris and bridge reconstruction;
- Importance index (I): The importance of a bridge at the time of operation depends on various parameters, such as the existence of alternative routes, the volume of daily trips on the bridge routes, the geometric conditions of the bridge bed (the possibility to quickly create temporary routes), the construction costs of the bridge, the structural characteristics of the bridge, the economic importance of the bridge, the importance of the bridge in terms of crisis management in special circumstances, etc. In this research, the population living near the bridge is used as a general indicator to determine the importance of the bridge.

$$R = (P + I)/2 \quad (3)$$

In this sense, Equation (4) calculates the reconstruction time index.

$$P = Normalize(Log_{10}(CON \times L \times W)) \quad (4)$$

where L is the length of the bridge; W is the width of the bridge, and CON is the reconstruction factor for the unit area of the bridge. The coefficient CON has different values for different bridge structures, as reported in Table 5.

Table 5. CON values according to the type of bridge structure.

Type of Bridge Structure	Coefficient CON
Simple	0.50
Steel	0.80
Concrete Slab–Steel Girder	0.90
Concrete Slab–Steel Box	0.95
Concrete Slab	1.00
Concrete Slab Box	1.20

In the end, the prepared databank in this study includes the following fields:

- The name of the bridge;
- Geographic coordinates of the bridge;
- Type of bridge structure (type of fragility function);
- Bridge worth (value);
- IDR coefficient to calculate the indirect damage of the earthquake according to the direct damage in each bridge.

7. Scenario Earthquakes

The ten-thousand-year catalog of earthquakes used in this study is based on a comprehensive database containing all possible seismic scenarios for the Tehran region. This database is an artificial earthquake catalog created by Zolfaghari (2014) using the Monte Carlo simulation approach and contains 84,000 independent earthquakes (Figure 2) [13]. Each of these scenarios contains the magnitude, geographic location, focal depth, and geometric features of the fault. Such a catalog provides a complete distribution of events in time, space, and magnitude. However, its implementation for risk analysis and damage assessment studies requires high computational power, especially when other sources of uncertainty are included in the calculations.

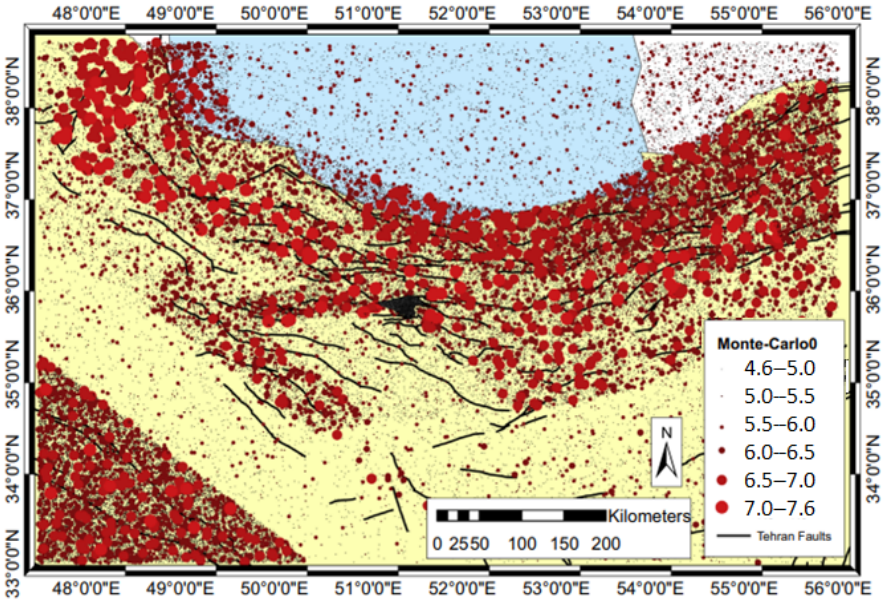

Figure 2. Synthetic catalog produced for Tehran [13].

The catalog prepared by Zolfaghari (2014) is based on the model of seismic areas in Tehran province. The seismic sources and seismic parameter values are listed in Figure 3 and Table 6, respectively [13].

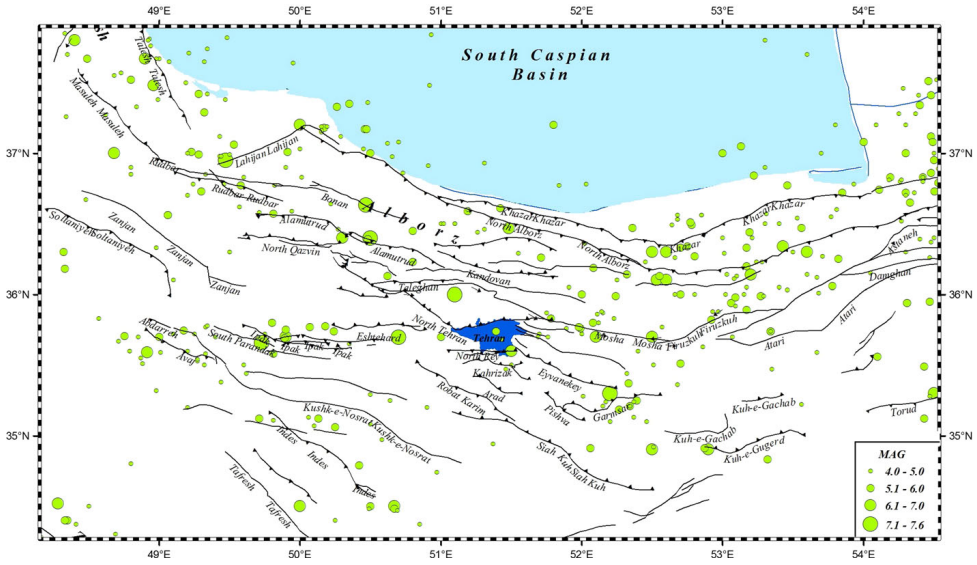

Figure 3. Seismic sources are used to generate a synthetic catalog [13].

Table 6. Characteristics of seismic sources in Tehran, [13].

Source	*a* Value (G-R)	*b* Value (G-R)	$N/(M \geq 4.0)$ per year	M_{max}
1	3.17	0.84	0.561	6.9
2	3.46	1.00	0.120	6.8
3	4.64	1.10	6.927	7.3
4	3.46	0.98	0.055	6.2
5	2.99	1.00	0.765	6.0
6	3.47	1.00	0.606	6.0
7	3.07	1.03	0.912	6.3
8	4.52	1.10	1.343	7.5
9	4.30	1.10	1.788	7.3
10	4.40	1.10	1.399	7.4
11	4.54	1.10	0.848	7.0
12	2.58	0.86	0.278	6.3
13	4.50	1.10	1.877	7.0
14	4.22	1.02	3.251	7.0
15	2.67	0.96	0.299	6.0
16	2.61	1.01	0.074	6.0
17	2.90	1.00	0.099	6.7
18	2.71	0.83	1.050	7.0
19	4.30	1.10	1.423	7.3
20	3.50	1.00	0.352	7.2
21	3.63	0.97	0.768	6.4
22	4.30	0.10	1.641	7.6
23	3.07	0.80	1.193	6.8
24	2.95	0.90	0.347	6.1

In order to study the seismic risk in bridges, all existing seismic scenarios should be considered. On the other hand, each of these scenarios should be considered as a unique event. Only in this case is it possible to claim that there is a spatial correlation between the values of ground motions in a given area, while overestimation of these values would be avoided in the analysis. Although considering all possible earthquakes in the seismic analysis offers numerous advantages, the analysis process then becomes time-consuming and tedious. Therefore, the approach of selecting scenarios and estimating probabilities based on the optimization method was used in this study. In addition, the seismic hazard with a return period of 475 years (10% in 50 years) was set as a benchmark.

From the 84,000 records proposed by Zolfaghari [13], 50 earthquakes were stochastically selected in this study, as shown in Figure 4. The catalog selected by the optimization-based probabilistic scenarios algorithm (OPS) was optimized to have the lowest error rate in the final risk curve in different regions of Tehran province compared to the original catalog.

In Figure 5, the seismic hazard of zones for an earthquake with a return period of 475 years (10% probability of exceedance in 50 years) is compared between the original catalog with 84,000 records and the reduced catalog with 50 records. Examination of the shape of the hazard curve in the two catalogs shows that the reduced catalog is a good representative of the original catalog.

Accordingly, the set of 50 ground motion records selected in this step is considered as an earthquake scenario. Since the synthetic catalog was extracted using seismic zones and the Gutenberg–Richter curve, each of these earthquakes is an independent event that does not correlate with the others. As a result, both the main catalog and the simulated catalog do not contain pre- or aftershocks.

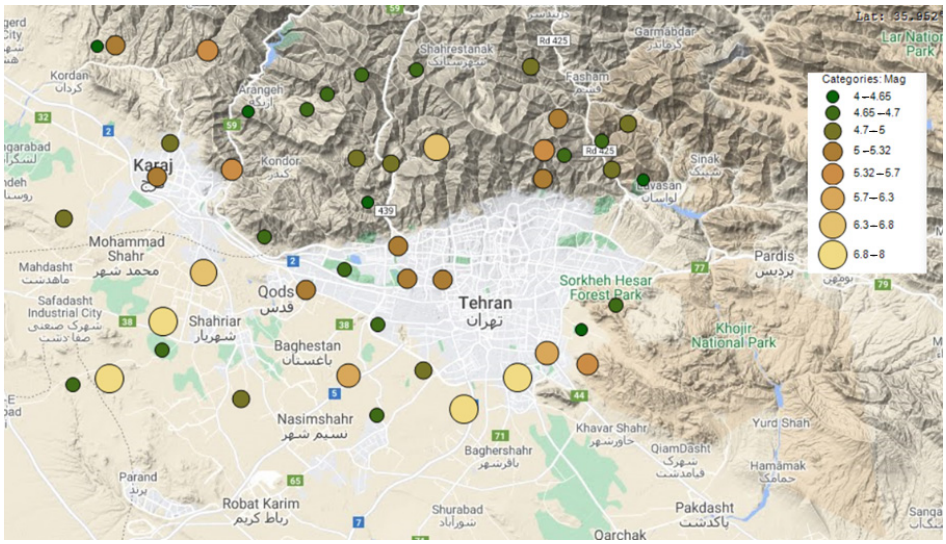

Figure 4. Filtered earthquake catalog including 50 earthquakes in Tehran province.

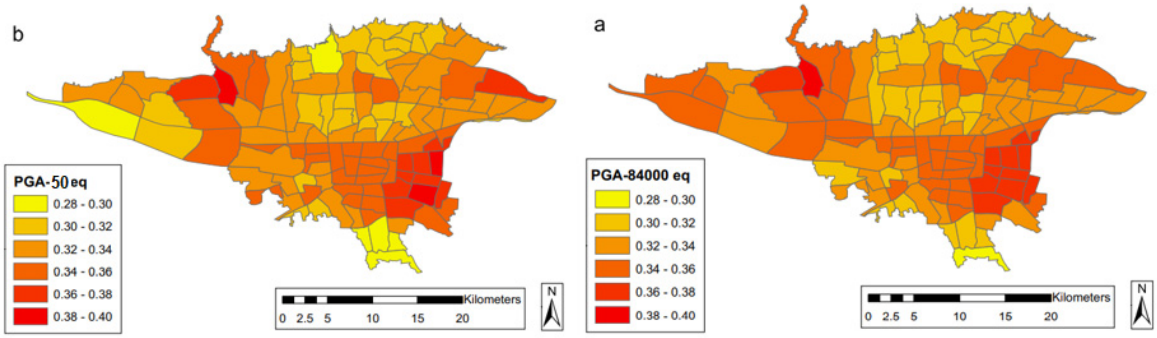

Figure 5. Comparison of the zone hazard risk between the original catalog (**a**) with the reduced one (**b**).

8. Seismic Risk Analysis of Bridges

One of the most effective factors in calculating earthquake risk is the selection of appropriate damping functions. There are a variety of relationships that can be used in this context. However, it is important that these relationships be consistent with the tectonic characteristics of the region and be able to take into account the most important parameters, such as the type of wave propagation path, the overall earthquake level characteristics, the area of the fault rupture, site specifications, etc. In this study, the NGA 2014 relations were used. In addition, an Iranian relation [14] was used to account for the local earthquake effect.

In order to eliminate the possible errors of attenuation relations in real studies and take advantage of the different relations, the logic tree method can be applied by assigning certain coefficients to each relation so that the probabilistic effects of all relations can be considered in estimating the final risk magnitude. The coefficients shown in Table 7 were used for each of these relations in this study.

Table 7. Impact coefficients in seismic risk estimation.

Relationship Title	Weight Coefficient
Abrahamson, Silva, 2014 [15]	1
Boore, 2014 [16]	1
Campbell, Bozorgnia, 2014 [17]	1
Chiou, Youngs, 2014 [18]	1
Idriss, 2014 [19]	1
Zare, 1999 [14]	1

In addition, in order to use the next-generation attenuation relations, the distance (several types of distances are required in each relation) must be calculated accurately. In particular, for larger earthquakes with high degrees of propagation, the exact characteristics of the fault rupture must be determined and the distance calculated on this basis. In this study, the rupture area for each of the earthquake scenarios was modeled as a rectangular 3-D plane, and its exact coordinates were calculated accordingly (Figure 6). The calculation process for the coordinates of the fault zone is as follows:

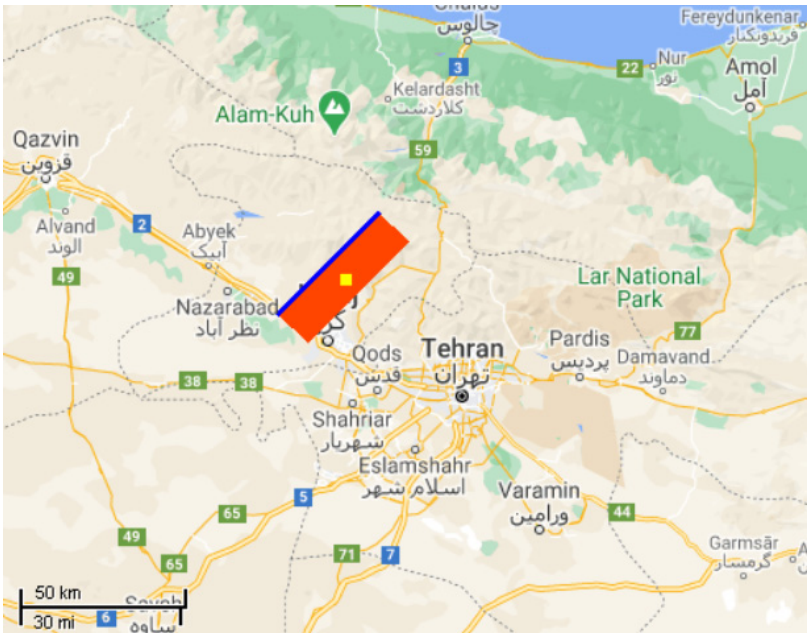

Figure 6. Calculation and 3-D plotting of the fault zone for all scenario earthquakes.

- Using the earthquake magnitude and empirical relationships, the length and area of the rupture are calculated (Table 8);
- Using the fault azimuth angle available in the simulated catalog, the fault zone is plotted with a center that coincides with the epicenter of the earthquake;
- Using the dip angle available in the simulated catalog and determining the depth of the fault zone, the 3-D plane of the fault zone is characterized.

Using the points where shear wave velocity is available (based on geographic coordinates), the value of shear wave velocity for any point is calculated using the linear IDW method. The linear interpolation method with IDW (Inverse Distance Weighting) is a common method in geophysics used to estimate data values at points where no measurements have been made. In terms of soil shear wave velocity, this method can help estimate and visualize the soil shear wave velocity in areas where direct measured data are not available.

The IDW method assumes that the nearest neighbors of the point of interest have the greatest influence on it. Based on this assumption, the value at each point is estimated according to its distance from the available data points and the weighting is calculated based on this distance. The general equation of IDW is as follows:

$$Z(x) = \frac{\sum_{i=1}^{n} w_i(x) \cdot Z_i}{\sum_{i=1}^{n} w_i(x)} \quad (5)$$

$Z(x)$ represents the value at the point x that you want to interpolate.

Z_i represents the value at data point i.

$w_i(x)$ is the weight corresponding to data point i at point x, calculated based on its distance from point x. This weight is usually the reciprocal of the distance to the second power of the reciprocal of the distance.

Table 8. Some empirical relations between fault rupture parameters and earthquake magnitude.

Fault	Equation	Standard Deviation	Reference
Strike-Slip	Log RL = −3.55 + 0.74M	σ_{logRL} = 0.23	1994-Wells and Coppersmith [20]
Reverse	Log RL = −2.86 + 0.63M	σ_{logRL} = 0.23	1994-Wells and Coppersmith [20]
Strike-Slip	Log RL = −4.10 + 0.80Ms	σ_{logRL} = 0.20	1984-Bonilla et al. [21]
Reverse	Log RL = −1.96 + 0.50Ms	σ_{logRL} = 0.20	1984-Bonilla et al. [21]
Strike-Slip	Log AD = −6.32 + 0.90M	σ_{logAD} = 0.28	1994-Wells and Coppersmith [20]
All	Log AD = −4.80 + 0.69M	σ_{logAD} = 0.36	1994-Wells and Coppersmith [20]
Strike-Slip	Log MD = −3.90 + 0.48Ms	σ_{logMD} = 0.26	1984-Bonilla et al. [21]
Strike-Slip	M = Log A + 3.98 for A $\leq$ 537km^2	σ_M = 0.03	2002-Hanks and Bakun [22]
	M = 1.33Log A + 3.07 for A > 537km^2	σ_M = 0.04	

Note: RL represents rupture length (km); AD is average displacement on the ground surface (m); MD is maximum displacement on the ground surface (m); A is rupture area (km^2). The base of all logarithms is 10. These relations cannot be applied to subduction zones.

The software developed in this study allows the shear wave velocity to be defined in terms of zone contours or discrete points (it can perform 3-D interpolations to calculate the shear wave velocity at any desired point). However, due to the lack of reliable information in this case, the shear wave velocity in this study was assumed to be constant and equal to 760 m/s. In addition, the soil amplification factor for the entire area was assumed to be 1.

The results for the peak ground acceleration (PGA) of the bridge exposed to recordings No. 1 and 10 are shown in Figures 7 and 8, respectively. It should be noted that the risk analysis process and PGA calculation for all bridges at each stage of the damage assessment and risk mitigation plan are performed by the software at high speed and for all earthquakes. The results shown in this section serve as examples for a better understanding of the process.

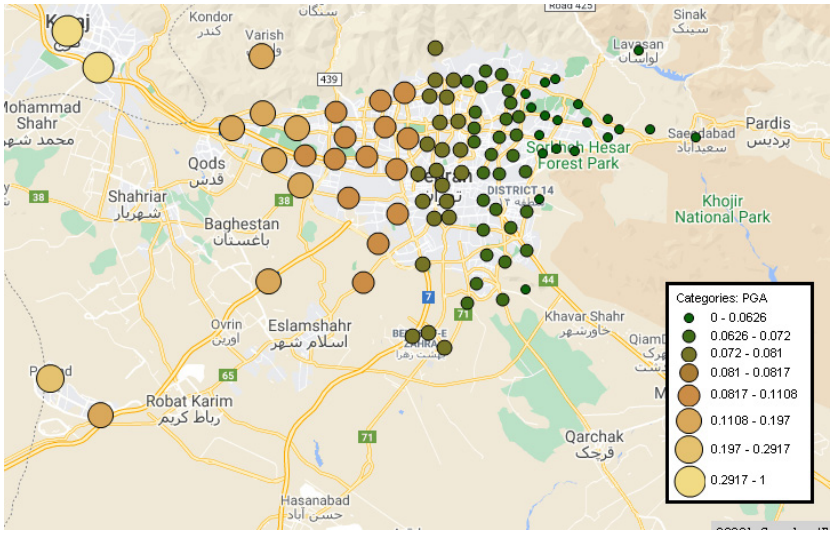

Figure 7. Acceleration in bridges, subjected to record No. 1 (magnitude of 7.2 on the Richter scale).

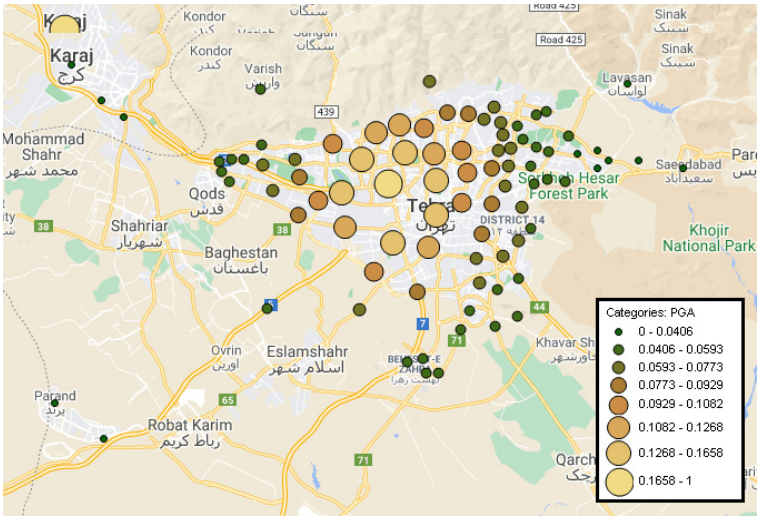

Figure 8. Acceleration in bridges, subjected to record No. 10 (magnitude of 5.4 on the Richter scale).

In fact, risk is defined as the product of risk (H) and vulnerability (V) in the inventory value (E), as expressed in Equation (6).

$$R = H(Hazard) \times V(Vulnerability) \times E(Exposure\ of\ Individuals\ or\ Assets) \quad (6)$$

9. Bridge Fragility Curve Generation Data

Considering that there are different types of bridges all over the world with different structural systems and years of construction, it is very difficult to find a fragility curve that expresses the vulnerability probability of a wide range of bridges. Moreover, it is obvious that each bridge was designed and built according to the regulations of the same country and the existing earthquake vulnerability. To solve this problem in this work, an importance coefficient was assigned to each of the generated fragility curves based on the previous work and the extraction of fragility curves for different structural systems according to the structural specifications and design regulations. Then, decision tree analysis was used to develop the overall fragility curves for each of the structural systems in the two states of bridge, i.e., age less than or greater than 10 years. Table 9 summarizes some of the references used in the logic tree modeling.

Table 9. List of references that develop bridge fragility curves, whose data was used in decision tree modeling in this study.

No.	Reference	Year	Region	Approach
1	(Avşar, 2011) [23]	2011	Turkey	Analytical–Nonlinear Dynamic
2	(Azevedo et al., 2010) [24]	2010	Portugal	Analytical–Nonlinear Static
3	(Naseri et al., 2020) [25]	2022	Iran	Analytical–Nonlinear Dynamic
4	(Mander and Basöz, 1999) [26]	1999	USA	Empirical–Analytical–Nonlinear Static
5	(Choi and Jeon, 2003) [27]	2003	USA	Analytical–Nonlinear Static
6	(Chang et al., 2012) [28]	2012	USA	Empirical and Analytical–Nonlinear Dynamic
7	(Li et al., 2013) [29]	2013	USA	Analytical–Nonlinear Dynamic
8	(Borzi et al., 2015) [30]	2015	Europe	Analytical Nonlinear Dynamic
9	(Karakostas et al., 2006) [31]	2006	Greece	Analytical–Nonlinear Static
10	(Yamazaki et al., 2000) [32]	2000	Japan	Empirical and Analytical–Nonlinear Dynamic
11	(Karim and Yamazaki, 2003) [33]	2003	Japan	Analytical–Nonlinear Dynamic
12	(Kibboua et al., 2017) [34]	2017	Algeria	Analytical–Nonlinear Dynamic
13	(Zourgui et al., 2018) [35]	2018	Algeria	Analytical–Nonlinear Dynamic
14	(Lupoi et al., 2005) [36]	2005	Europe	Analytical–Nonlinear Dynamic
15	(Moschonas et al., 2009) [37]	2009	Greece	Analytical–Nonlinear Static

Table 9. *Cont.*

No.	Reference	Year	Region	Approach
16	(Nielson and DesRoches, 2007) [38]	2007	USA	Analytical–Nonlinear Dynamic
17	(Nielson 2005) [39]	2005	USA	Analytical–Nonlinear Dynamic
18	(Padgett and DesRoches, 2009) [40]	2009	USA	Analytical–Nonlinear Dynamic
19	(Naseri et al., 2017) [41]	2017	Iran	Analytical–Nonlinear Dynamic
20	(Pan et al., 2010) [42]	2010	USA	Analytical–Nonlinear Dynamic
21	(Shinozuka et al., 2000) [43]	2000	Japan	Empirical and Analytical–Nonlinear Dynamic
22	(Banerjee and Shinozuka, 2007) [44]	2007	Japan	Analytical–Nonlinear Static
23	(Shirazian et al., 2011) [45]	2011	Iran	Analytical–Nonlinear Dynamic
24	(Yi et al., 2007) [46]	2007	USA	Analytical–Nonlinear Dynamic
25	(Rezaei et al., 2022) [47]	2022	Iran	Analytical–Nonlinear Dynamic
26	(Lee et al., 2007) [48]	2007	Korea	Empirical and Analytical–Nonlinear Dynamic
27	(Zakeri et al., 2014) [49]	2014	USA	Analytical–Nonlinear Static
28	(Noori et al., 2016) [50]	2016	Iran	Analytical–Nonlinear Static
29	(M.Goltabar.R et al., 2018) [51]	2018	Iran	Analytical–Nonlinear Dynamic
30	(Pahlavan et al., 2016) [52]	2016	Iran	Analytical–Nonlinear Dynamic
31	(Ren et al., 2019) [53]	2019	China	Analytical–Nonlinear Dynamic
32	(Hwang et al., 2001) [54]	2001	USA	Analytical–Nonlinear Dynamic
33	(Naseri et al., 2020) [55]	2020	Iran	Analytical–Nonlinear Dynamic
34	(Mosleh, 2016) [3]	2016	Iran	Analytical–Nonlinear Dynamic
35	(Moschonas et al., 2009) [37]	2011	Greece	Analytical–Nonlinear Dynamic
36	(Choi, 2002) [27]	2002	USA	Analytical–Nonlinear Dynamic
37	(Riga et al., 2019) [56]	2019	Greece	Analytical–Nonlinear Dynamic
38	(Karimi-Moridani et al., 2017) [57]	2017	Iran	Analytical–Nonlinear Dynamic
39	(Esfandiar and Khorraminejad 2017) [58]	2017	Iran	Analytical–Nonlinear Dynamic
40	(Billah et al., 2013) [59]	2013	USA	Analytical–Nonlinear Dynamic
41	(Kaynia et al., 2013) [60]	2013	Europe	Empirical and Analytical–Nonlinear Dynamic
42	(Ramanathan, 2012) [2]	2012	USA	Analytical–Nonlinear Dynamic
43	(Shinozuka et al., 2000) [43]	2000	Japan	Analytical–Nonlinear Static
45	(Jeong and Elnashai, 2007) [61]	2006	Korea	Analytical–Nonlinear Dynamic
47	(Pahlavan et al., 2016) [52]	2016	USA	Analytical–Nonlinear Dynamic
48	(Naseri et al., 2017) [41]	2017	USA	Analytical–Nonlinear Dynamic
49	(Feng et al., 2000) [62]	2000	Japan	Empirical and Analytical–Nonlinear Dynamic
50	(Saxena, 2000) [63]	2000	USA	Analytical–Nonlinear Dynamic
51	(Balou et al., 2022) [64]	2022	Iran	Analytical–Nonlinear Static
52	(Kaveh et al., 2021) [65]	2021	Iran	Analytical–Nonlinear Dynamic

10. Classification of Bridges of Tehran City

The city of Tehran has more than 400 highway intersections over which about 600 bridges have been built. The scattering of these bridges is plotted in Figure 9 over Tehran City. While studying the structure of these bridges, it was found that there are 72 types of frame structures for these bridges. Therefore, all bridge inventories were classified into six main groups: simple, steel, concrete slab box, concrete slab–steel box, concrete slab, and steel girder–concrete slab. The main framing parameters used in generating the fragility curves included the bridge material, the number of piers and spans, the type of structure, and the design method. The structural details of the bridge frames used in this study are summarized in Table 10.

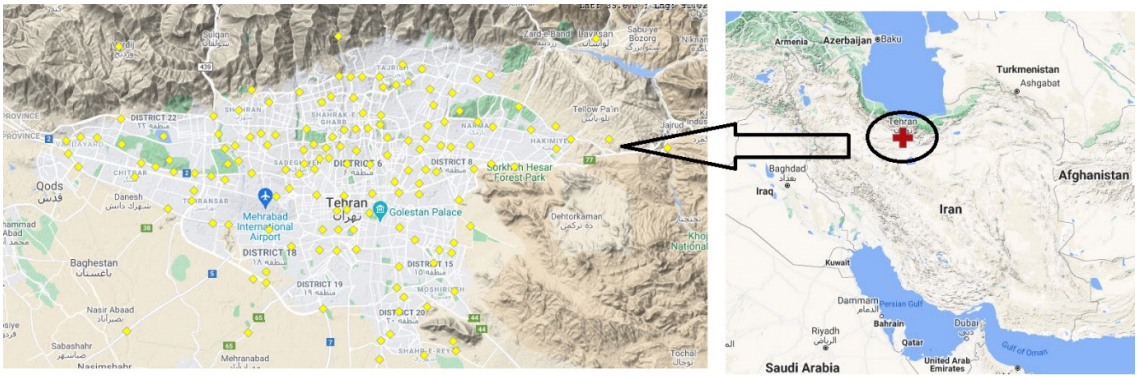

Figure 9. Scatter map of highway bridges across Tehran City [66].

Table 10. Structural details of bridges across Tehran City [66].

Bridge Component		Percentage (%)
Deck Area	<1000 m^2	24
	1000–4000 m^2	61
	>4000 m^2	15
Material	Concrete	91
	Steel	9
Column Height	<10 m	88
	>10 m	12
Functional Importance	Essential	90
	Standard	10
Residual Expected Lifetime	0–15 (years)	45
	16–50 (years)	40
	>50 (years)	15
Deck Supports	Simple	12
	Continuous	88

11. Classification of Bridge Fragility Curves

To obtain weight coefficients, previous research designs available in the literature were compared with the frame designs of bridges in Tehran city in the process of decision tree analysis. Table 11 shows the derived weight coefficients for each bridge type and component. They range from 0 to 1 and were selected based on engineering judgments. In this context, for the steel girder–concrete slab bridge type, a coefficient of 0.2 was determined for the concrete or steel material. However, for the same bridge type, a coefficient of 0.6 was chosen for the composite material. Additionally, weight coefficients of 0.4 and 0.6 were considered for this bridge type when the bridge includes either a single span or multiple spans. In the past, most of Tehran's bridges were built when seismic codes were not generally included in structural codes. In this sense, the weight coefficients of 0.33 and 0.67 were established for bridges with and without seismic design approaches, respectively. In addition, 0.3 and 0.7 were assigned to simple and continuous columns, respectively.

Despite the similarity in design approaches, different regulations and implementations are applied in different countries, which significantly affects the seismic safety of bridges and the associated fragility curves. In this study, different sources of information from different countries around the world were selected to obtain a more robust analysis. Table 12 provides weighting coefficients ranging from 0 to 1 for different countries selected based on the similarity of their bridges to the bridges in the city of Tehran. For example, Turkey was assigned a weighting coefficient of 1 because their bridges are similar to the bridges in Tehran in terms of design approach, structural details, implementation techniques, and engineering principles. However, lower values were assigned for areas with less similarity.

For example, the weighting coefficient for Europe, where there is less ground motion, was set at 0.5.

Table 11. Derived weight coefficients for each bridge type and component used in this study [66].

		Concrete Slab Box	Concrete Slab	Concrete Slab–Steel Box	Steel Girder–Concrete Slab	Steel	Simple
Material	Concrete	1	1	0.2	0.2	0	0.5
	Steel	0	0	0.2	0.2	1	0.5
	Composite	0	0	0.6	0.6	0	0
Span Number	Multi–Span	0.6	0.6	0.6	0.6	0.6	0.6
	Single–Span	0.4	0.4	0.4	0.4	0.4	0.4
Pier Number	Multi–Column	0.6	0.6	0.6	0.6	0.6	0.6
	Single–Column	0.4	0.4	0.4	0.4	0.4	0.4
Design Approach	Seismic	0.7	0.67	0.75	0.7	0.6	0.4
	No Seismic	0.3	0.33	0.25	0.3	0.4	0.6
Support Type	Continuous	0.7	0.7	0.7	0.7	0.6	0.4
	Simple	0.3	0.3	0.3	0.3	0.4	0.6

Table 12. Weight coefficients for different countries were chosen based on their design similarities with bridges across the city of Tehran [66].

Region	Value
Turkey	1
Portugal	0.6
US	0.7
Greece	0.8
Europe	0.5
Japan	0.6
Korea	0.8
Algeria	1
Iran	1

Further classification of the bridge fragility curves was made according to the analytical approach used in the extraction. Accordingly, four methods were used to develop bridge fragility curves, including the physical-based, static nonlinear, dynamic nonlinear, and coupled physical-based dynamic nonlinear approaches. The application of each method has a significant effect on the estimation accuracy in the evolution of the fragility curve. In this regard, the physical-based approach is very accurate because it relies on real ground motion records from the past. The dynamic nonlinear approach also provides fairly accurate results. Table 13 lists the weighting coefficients ranging from 0 to 1 for each of the analytical approaches discussed. It should be noted that higher values show higher accuracy of the approach and greater similarity to reality.

Table 13. Weight coefficients for each of the analytic approaches [66].

Extraction Methods of Fragility Curves	Value
Analytic (dynamic non-linear)	0.8
Analytic (static non-linear)	0.7
Experimental	0.6
Experimental + Analytical (dynamic non-linear)	1
Experimental + Analytical (static non-linear)	0.9

12. Extracting Fragility Curves

The weight coefficients discussed in the previous section were coupled with the logic tree algorithm to extract the fragility curves of Tehran bridges. Figure 10 shows the fragility curves with PGA on the x-axis and probability of damage state exceedance (PDSCE) on the

y-axis for different bridge systems of age more or less than 10 years at different damage states (slight, moderate, extensive, and complete). Once different sources of uncertainty were included in the decision tree algorithm, the fragility curves were plotted. The obtained curves were then reused in the logic tree analysis to generate new fragility curves for bridges in Tehran city.

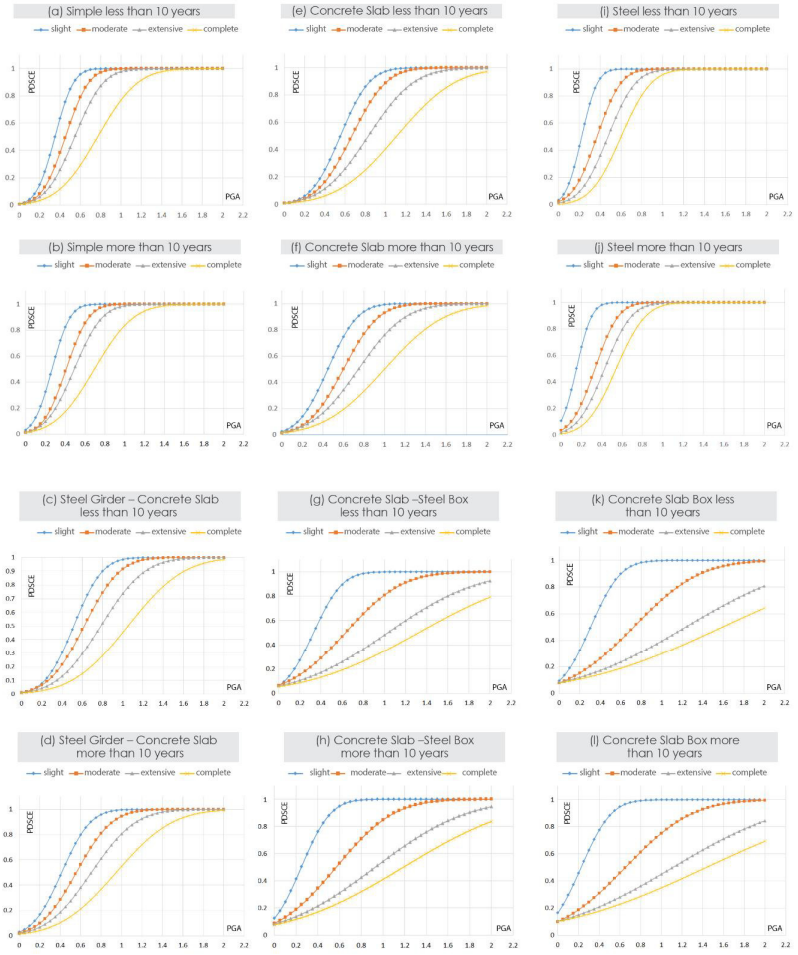

Figure 10. Fragility curves for different bridge systems at different ages and various damage states [66].

13. Case Study Application

To evaluate the accuracy of extracted fragility curves via the logic tree algorithm in the present study, a case study of a bridge older than 10 years, located at the intersection of Motahari Street and Modarres Highway in downtown Tehran, was selected, as shown in Figure 11.

Figure 11. Case study bridge at the intersection of Motahari Street and Modarres Highway in downtown Tehran [66].

There are several methods for generating structural fragility curves, including experimental, analytical, or engineering assessment methods [67], with the analytical method being used. The structural system of this bridge is a concrete slab box girder with two separated carriageways and expansion joints in between. Thus, the bridge consists of two spans, each 15 m long. The total length and width of the deck are 31 and 31 m, respectively. Each of the decks includes three lanes with an inclination of 12°. The height of the piers varies between 6.7 and 7.3 m, and the height of the piers ranges between 4.9 and 5.5 m. The length of the foundation in the center (under the piers) is 33 m with a base width of 6 m. The foundations of the abutments are 33 m long and 5.05 m wide. Figure 12 outlines the geometrical characteristics of the case study bridge.

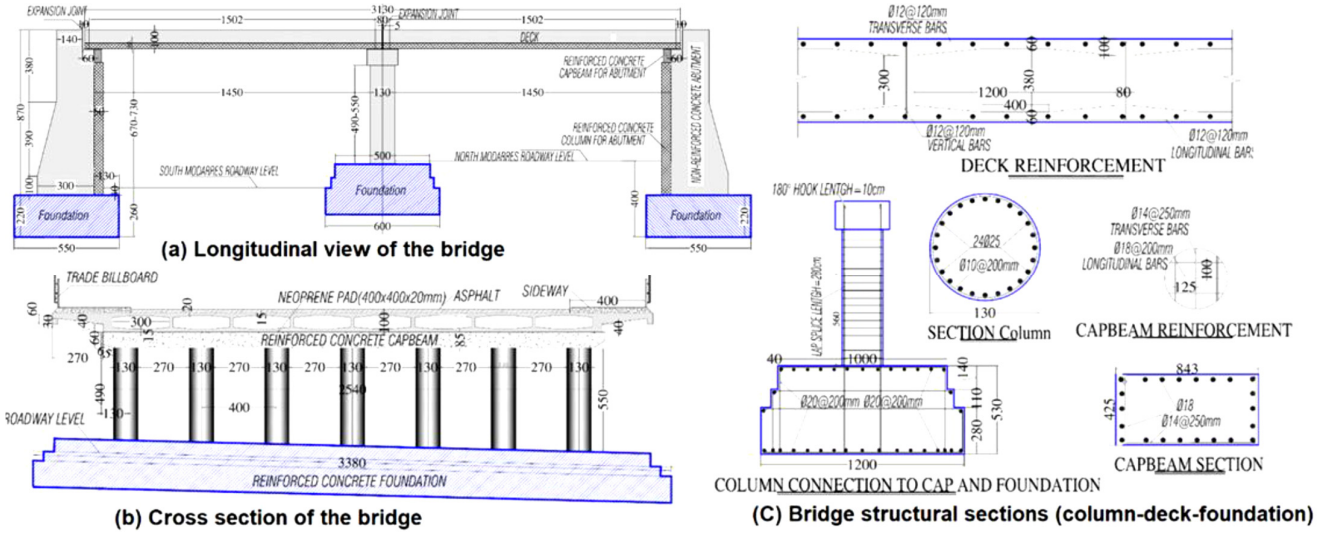

Figure 12. Geometric details of the case study bridge [63].

A set of ground motion records representing the risk of excitation in the studied region was selected to perform the analysis. All records had a magnitude between 6 and 8 on the Richter scale and an epicenter distance greater than 8 km. According to Shome [68], a set of 10–20 records can be considered adequate to perform the analysis. Therefore, a total of 20 ground motion records (Table 14) were selected for the present study from the PEER Ground Motion database [41] and the records available in the Iranian database.

Figure 13 demonstrates the varying responses of various bridge components modeled by Naseri et al. (2022) via OpenSEES [6]. For a detailed examination of the bridge component modeling process, Mogheisi et al. (2023) [66] can be referred to.

Table 15 describes how to model each bridge component in OpenSEES software.

The comparison of the results of the fragility curve from the tree analysis, based on previous studies in the literature, and the case study of the bridge and modeling in the OpenSEES software is shown in Figure 14. In this figure, model (1) shows the results of decision tree analysis, and model (2) shows the results of incremental dynamic analysis (IDA). Based on the results of the two modeling approaches, the fragility curves almost coincide for a small amount of damage for PGAs below 0.4 g. However, there is an average difference of 8% between the two methods when the PGAs are larger than 0.4 g. At moderate levels of damage, the corresponding discrepancy is about 10% for PGAs less than 0.8 g, after which the difference in fragility measures increases to 15%. Similarly, at the extensive damage level, the difference in results between the two models was negligible for PGAs below 0.3 g and 22% for PGAs above 0.3 g. Finally, at the extensive damage level, the results were close up to PGAs of less than 0.3 g, after which the difference increased to 18%.

Table 14. Earthquake records used in the analysis [41].

ID NO.	Earthquake			Station Name	NEHRP Class	PGA Max (g)
	M	Year	Name			
R1	6.7	1994	Northridge	Beverly Hills-Mulhol	D	0.52
R2	6.7	1994	Northridge	Canyon Country-WLC	D	0.48
R3	7.1	1999	Duzce, Turkey	Bolu	D	0.82
R4	7.6	1999	Chi-Chi, Taiwan	WGK	D	0.334
R5	6.5	1979	Imperial Valley	Delta	D	0.35
R6	6.5	1979	Imperial Valley	El Centro Array #11	D	0.38
R7	6.5	1979	Imperial Valley	6619 SAHOP Casa Flores	D	0.506
R8	6.9	1995	Kobe, Japan	Shin-Osaka	D	0.24
R9	7.5	1999	Kocaeli, Turkey	Duzce	D	0.36
R10	7.4	1978	Tabas, Iran	71 Ferdows	D	0.108
R11	7.3	199	Landers	Yermo Fire Station	D	0.24
R12	7.3	199	Landers	Coolwater	D	0.42
R13	6.9	198	Loma Prieta	Capitola	D	0.53
R14	6.9	1989	Loma Prieta	Gilroy Array #3	D	0.56
R15	7.4	1990	Manjil, Iran	BHRC Tonekabun	D	0.11
R16	6.5	1987	Superstition Hills	El Centro Imp. Co.	D	0.36
R17	6.5	1987	Superstition Hills	Poe Road (temp)	D	0.45
R18	7	1992	Cape Mendocino	Rio Dell Overpass	D	0.55
R19	7.6	1999	Chi-Chi, Taiwan	CHY101	D	0.44
R20	6.6	1971	San Fernando	LA-Hollywood Stor	D	0.21

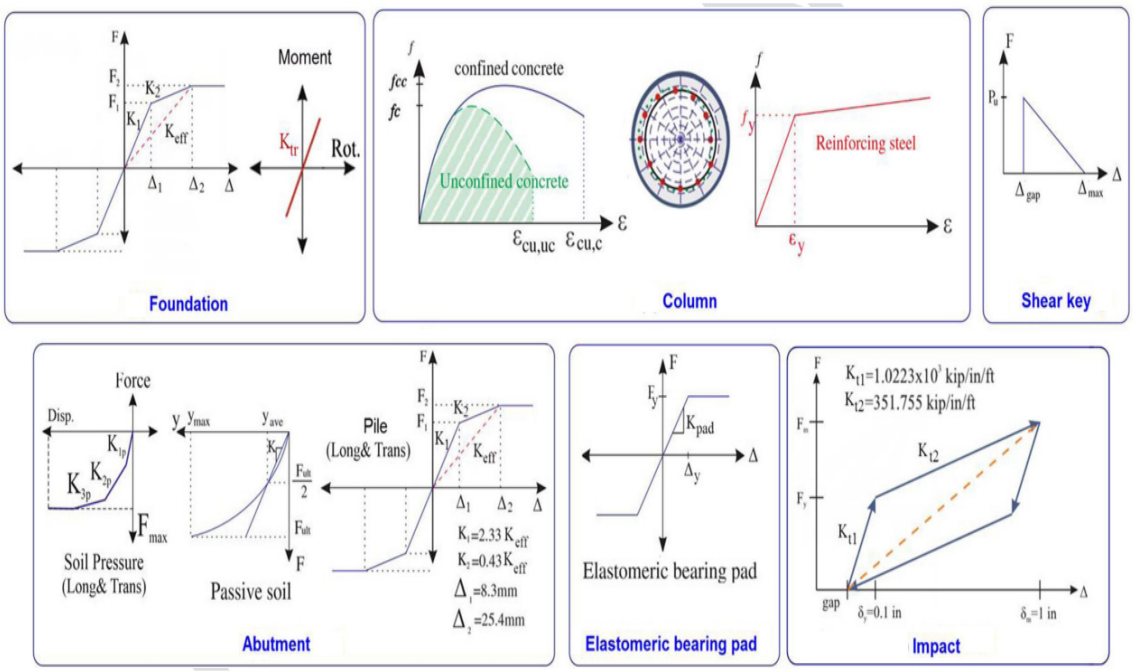

Figure 13. Non-linear responses of various bridge components modeled in OpenSEES [6].

Table 15. Behavior of different bridge components and modeling in OpenSEE [25].

Bridge Component or Material	Modeled Element Type and Behavior
Deck	Elastic beam-column element with calculated section properties
Column	Nonlinear beam-column element with fiber section
Elastomeric bearings	Elastic-perfectly-plastic behavior with steel 01 material applied to zero-length element
Impact	Bilinear behavior applied to zero-length element
Piles	Uniaxial material hysteretic with trilinear behavior
Abutment	Hyperbolic gap material with parabolic soil behavior applied to zero-length element
Shear key	Uniaxial hysteretic behavior applied to zero-length element
Concrete	Concrete 07 material with monotonic stress-strain characteristic
Reinforcing steel bars	Steel 02 material with isotropic strain-hardening behavior

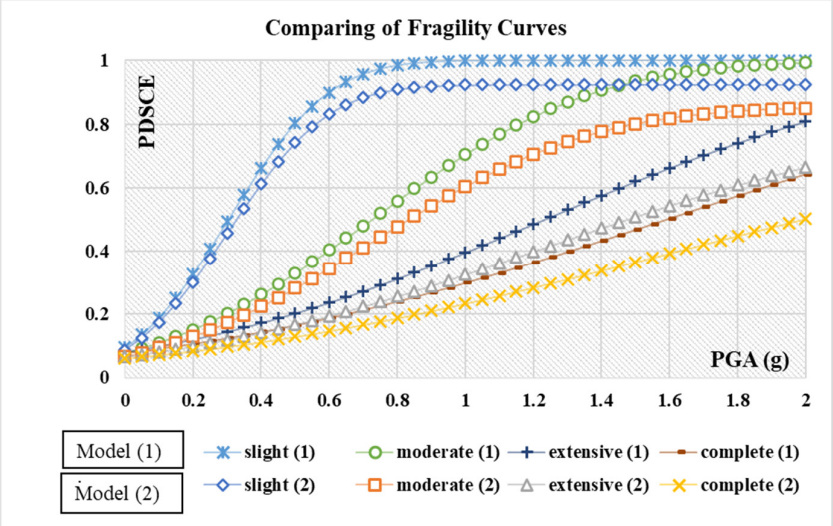

Figure 14. Comparison of the fragility curve results between model (1): obtained from decision tree analysis and model (2): extracted from IDA modeling.

14. Estimating Seismic Damage in Bridges

The probability of the bridge being slightly, moderately, extensively, and completely damaged after an earthquake in any of the states is calculated using the fragility functions. The estimated values are then normalized so that the sum of the probabilities in the four states equals one. In other words, it can be concluded that the bridge can only assume one of the above damage states after an earthquake. It should be noted that the "slight damage" state also covers the probability of the "no damage" state of the bridge.

The following two steps are required to calculate the damage level:

- Calculation of earthquake risk (using ShakeMap analysis);
- Definition of fragility relations corresponding to the type of structure defined in the bridge database.

The damage analysis can then be performed using these two values. The damage analysis results include four levels indicating the possible values of each damage level from slight, moderate, extensive, and complete, respectively [40,69].

Figures 15 and 16 show the damage estimation results for bridges exposed to earthquakes No. 1 (7.2 Richter) and No. 10 (5.4 Richter).

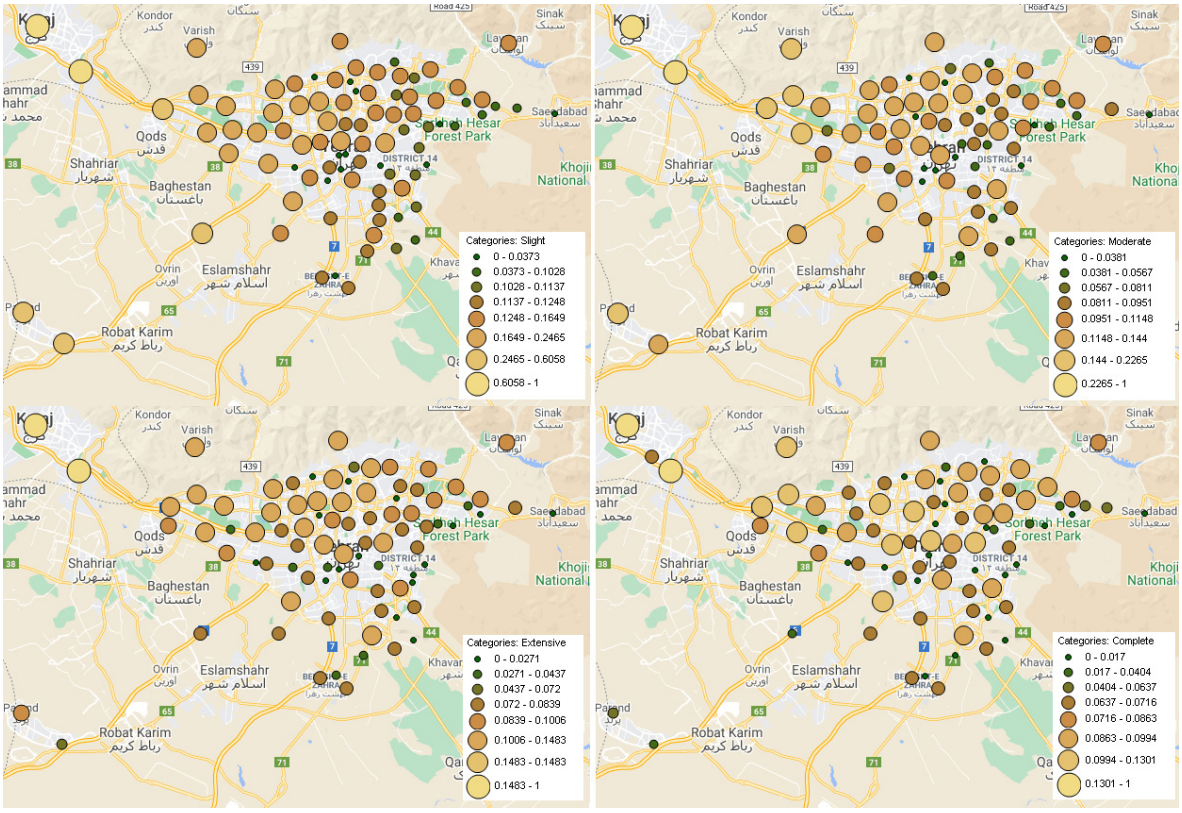

Figure 15. Earthquake No. 1 (7.2 Richter).

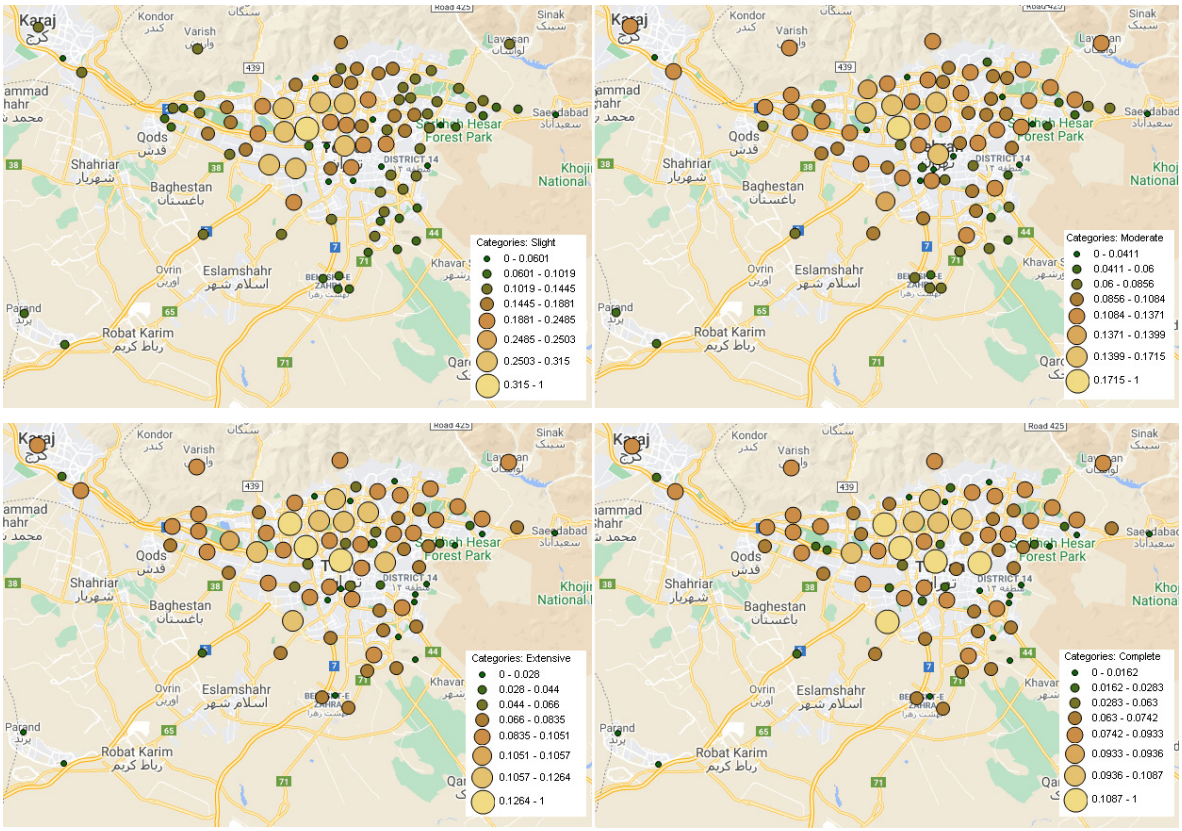

Figure 16. Earthquake No. 10 (5.4 Richter).

15. Estimating Damage Function

Direct damage caused by an earthquake includes physical destruction of buildings, damage to communication networks, and human death. In this study, direct damage is only concerned with damage to bridges. Thus, it is assumed that bridge damage does not result in fatalities.

To calculate the damage, the damage function must first be extracted. There are two solutions for this:

- Extraction of damage functions directly from damage recorded in past earthquakes;
- Extraction of damage functions based on fragility functions.

In this study, the second method was used. However, the functions extracted by the first method can also be used in the program proposed for the evaluation of seismic damage to bridges in this study. In this study, an equivalent damage of 10% to the bridge structure was assumed for a low level of damage. Similarly, damage amounts of 20, 30, and 40% were considered for moderate, extensive, and complete damage, respectively. Thus, Equation (7) applies to each point in the fragility function as follows:

$$Loss = 0.1 \times Slight + 0.2 \times Moderate + 0.3 \times Extensive + 0.4 \times Complete \quad (7)$$

In Equation (6), the parameters low, moderate, extensive, and complete represent the four levels of failure probability from low to complete, and the structural damage is calculated by applying coefficients according to their effect.

According to Equation (7), the risk functions based on PGA were plotted for the six studied bridge systems older than 10 years in Tehran city, as shown in Figures 17–22.

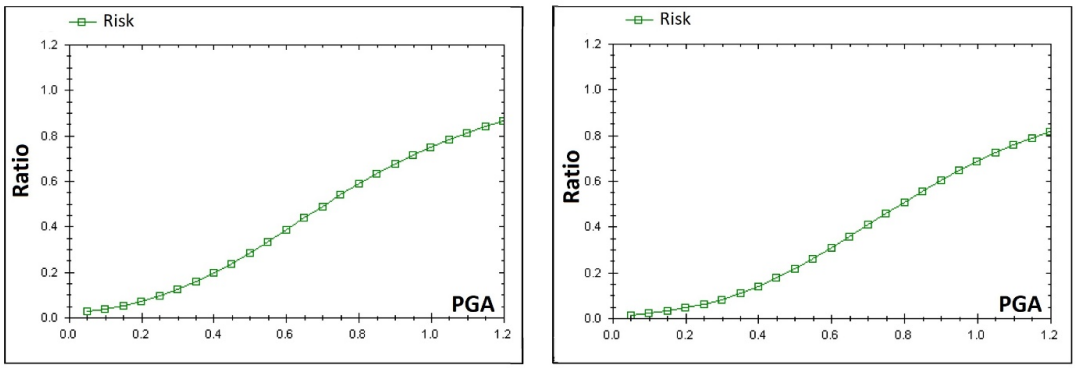

Figure 17. Risk functions of concrete slab box bridge aged (**a**) less than 10 years, and (**b**) more than 10 years.

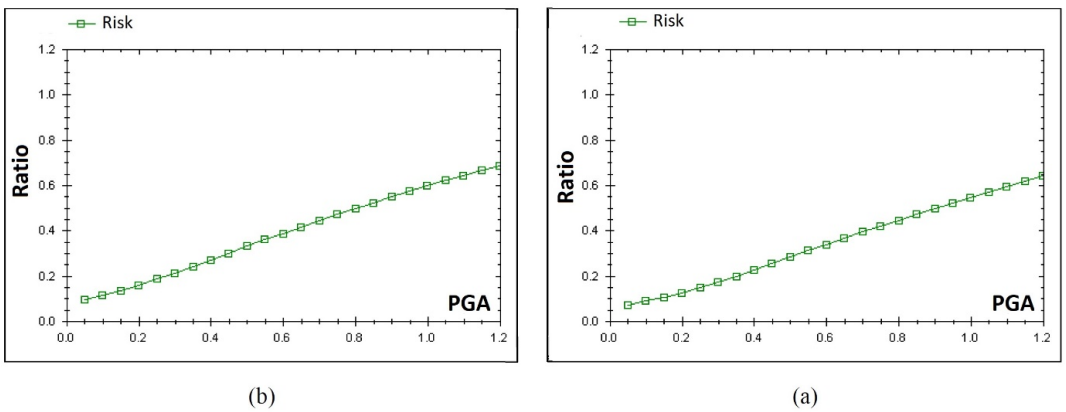

Figure 18. Risk functions of concrete slab bridge aged (**a**) less than 10 years, and (**b**) more than 10 years.

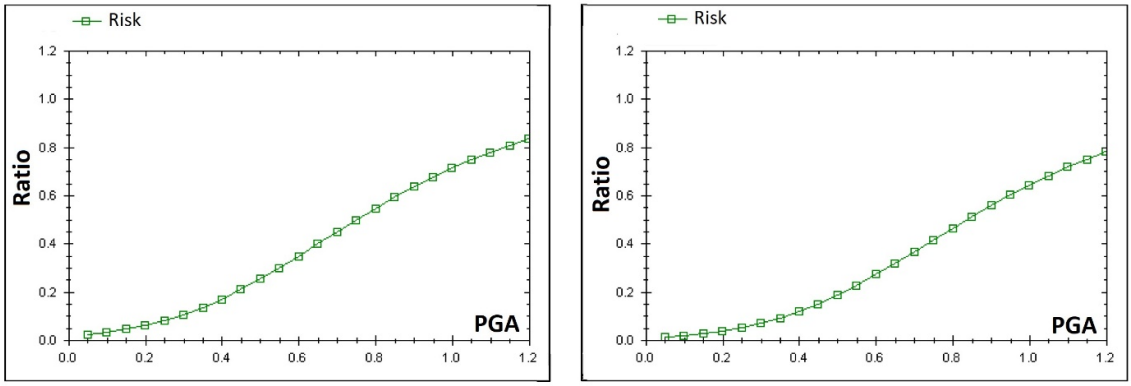

Figure 19. Risk functions of concrete slab–steel box bridge aged (**a**) less than 10 years, and (**b**) more than 10 years.

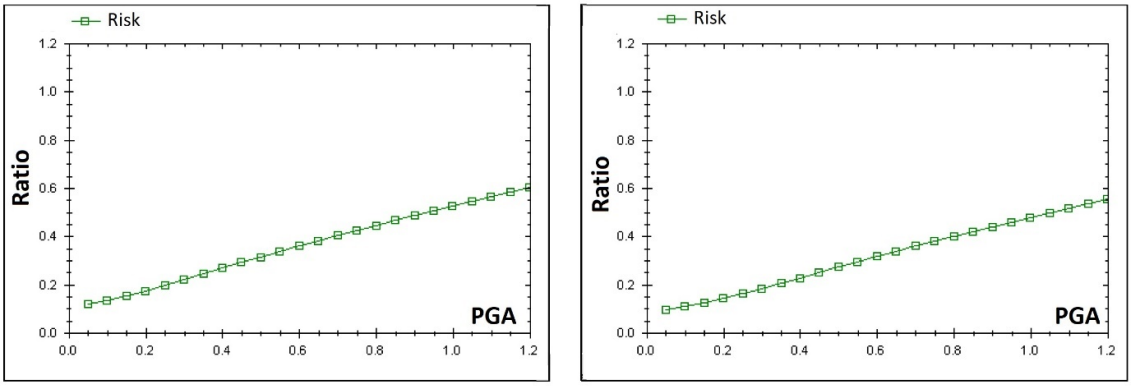

Figure 20. Risk functions of concrete slab–steel girder bridge aged (**a**) less than 10 years, and (**b**) more than 10 years.

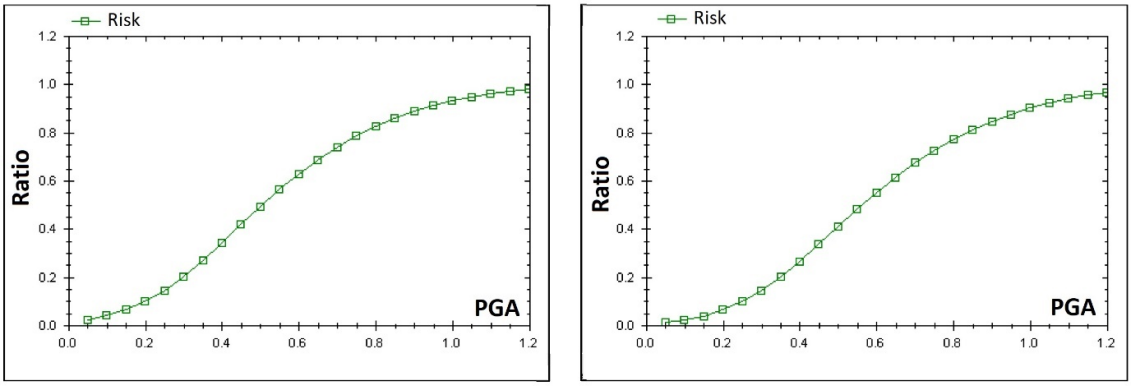

Figure 21. Risk functions of steel bridge aged (**a**) less than 10 years, and (**b**) more than 10 years.

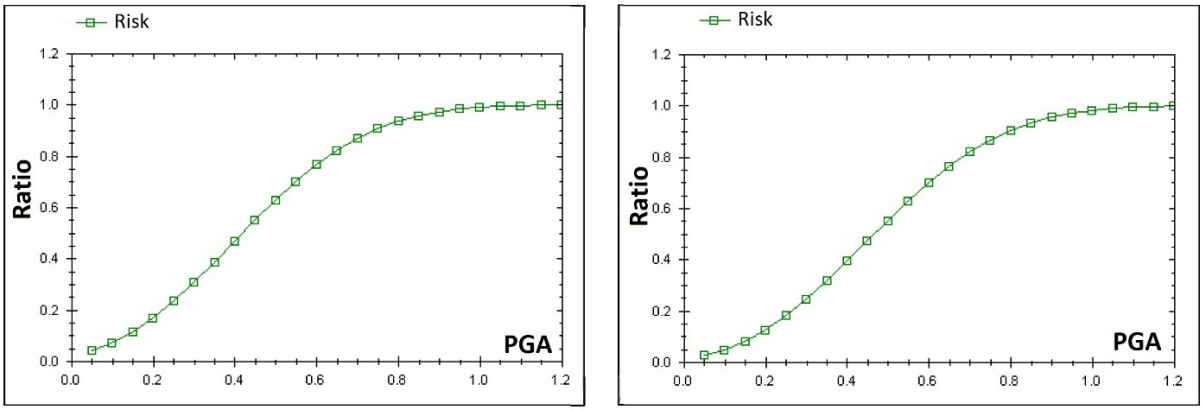

(b) (a)

Figure 22. Risk functions of simple bridge aged (**a**) less than 10 years, and (**b**) more than 10 years.

For a better comparison of damage function curves of all types of seismic systems of bridges aged less or more than 10 years, the median vulnerability of bridges (PGA at 50% probability of damage) was calculated as shown in Table 16 and Figure 23. The numbers 1 and 2 at the end of each bridge ID represent a bridge with an age of more than 10 years and a bridge with an age of less than 10 years, respectively.

Table 16. Median vulnerability values of different bridge systems with an age of less or more than 10 years.

Bridge ID	Median Vulnerability (PGA)
SBCD 1	0.71
SBCD 2	0.8
CD 1	0.78
CD 2	0.89
SSCD 1	0.75
SSCD 2	0.84
CS1	0.92
CS2	1.04
S1	0.49
S2	0.57
SIM 1	0.42
SIM 2	0.46

As can be seen, the median damage (PGA) in all cases for the bridge more than ten years old is between 0.85 and 0.9 times (on average 0.88) the median damage for the bridge less than ten years old.

This is an indication that the vulnerability of the bridge is increased. In this regard, the bridge with a simple structure is the most vulnerable, with a median value of 0.44. The lowest level of vulnerability corresponds to the bridge with a steel girder–concrete slab system with a median vulnerability of 0.98, which is about 2.2 times the median vulnerability.

As shown in Figure 23, bridges ranked in the order of simple, steel, concrete slab box, concrete slab–steel box, concrete slab, and steel girder–concrete slab systems have the highest vulnerability levels, in that order.

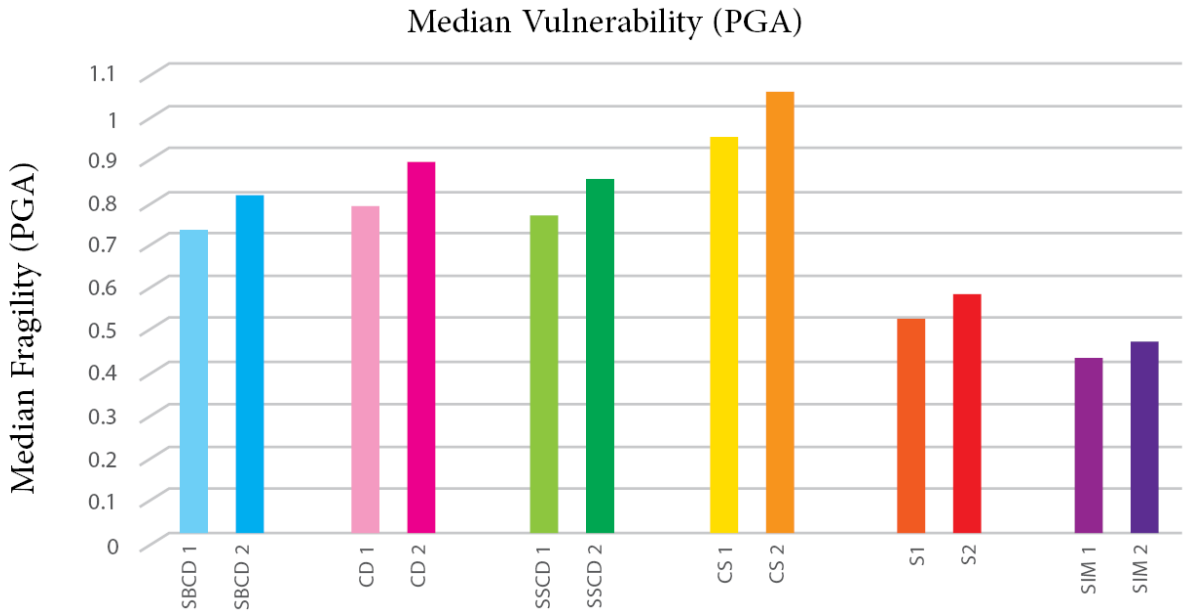

Figure 23. Median vulnerability values of different bridge systems with an age of less or more than 10 years.

Equation (8) can be applied to estimate the direct damage using the damage function.

$$Direct\ Loss = Value \times Loss\ Ratio \tag{8}$$

in which *Loss Ratio* represents a coefficient obtained from the damage function. A value also refers to the value of the asset, which in this case is the value of the bridge structure. The asset value in calculating the direct loss index is defined based on how much it costs to build a similar structure at present. Human casualties (if included) are usually valued based on blood money (if applicable).

The total damage can then be determined using Equation (9) by calculating the *IDR* (changing direct damage to indirect damage).

$$Loss = (1 + IDR) \times Direct\ Loss \tag{9}$$

According to the previous discussions, it is possible to calculate the extent of damage to bridges under any earthquake scenario. The results of damage estimation for bridges subjected to earthquakes No. 1 (7.2 Richter) and No. 10 (5.4 Richter) are shown in Figures 24 and 25, respectively.

It is worth noting that the main goal of this research is to provide a comprehensive risk reduction plan. This is where the economic risk calculation is considered as one of the modules of a risk reduction strategy. Therefore, the economic risk results have only been presented for earthquakes No. 1 and No. 10 in this section as examples. Obviously, it is possible to estimate and display the risk in the final software version for each earthquake scenario.

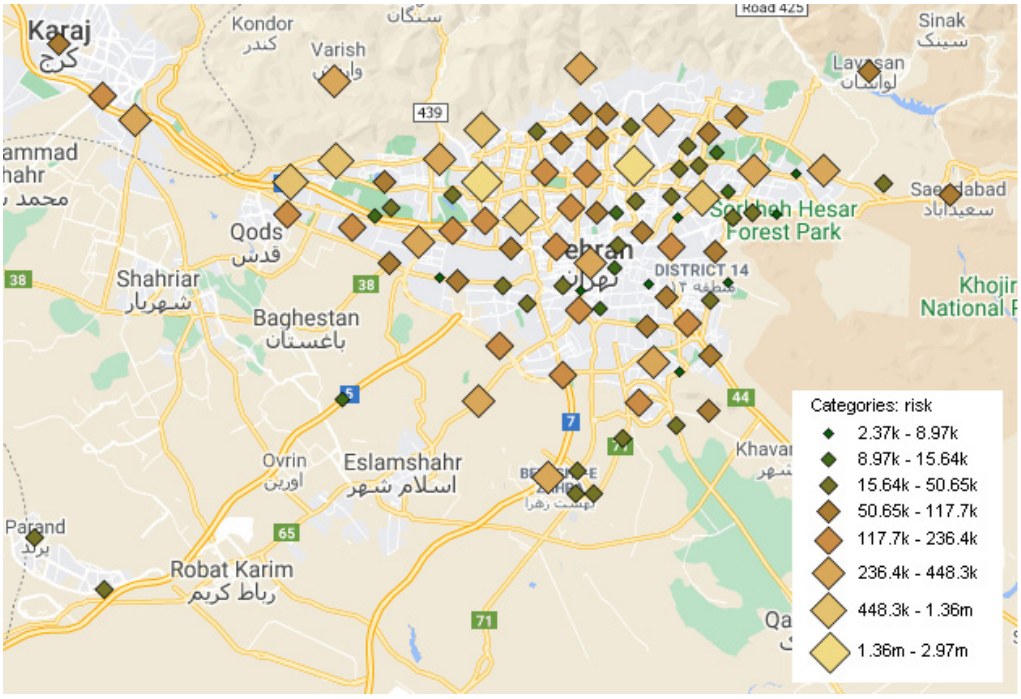

Figure 24. Earthquake No. 1 (7.2 Richter).

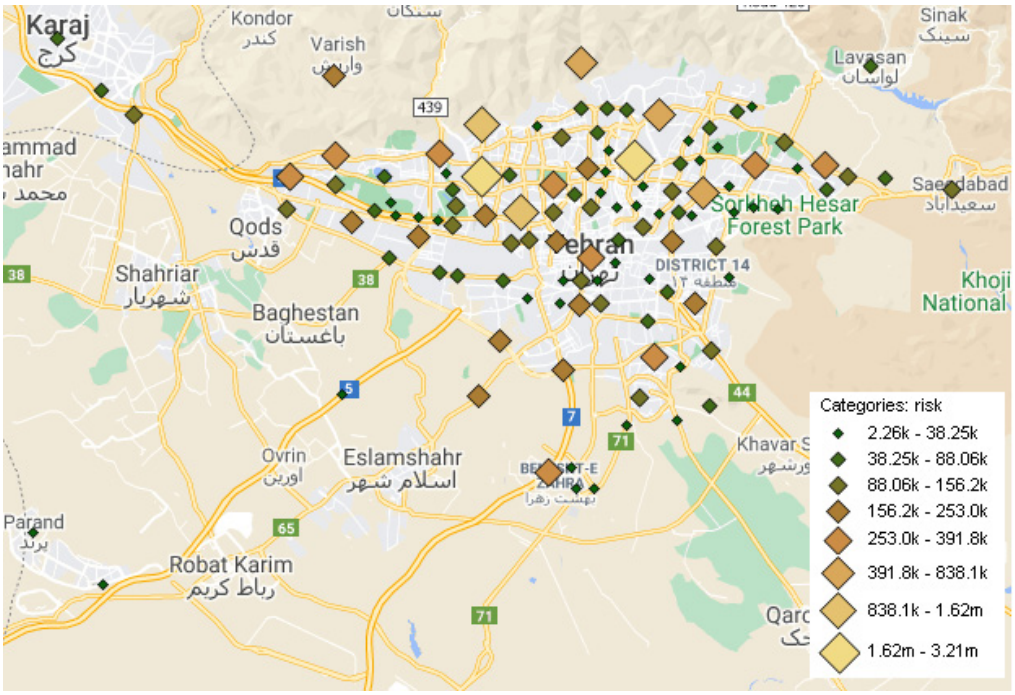

Figure 25. Earthquake No. 10 (5.4 Richter).

16. Sensitivity Analysis vs. Reconstruction Index

In this research, the CON index was used to express the effect of bridge reconstruction time on reducing indirect earthquake risk. This section investigates the effect of changes in this index on the amount of direct, indirect, and total risk. For this purpose, the reconstruction index was varied in the range of 0.005 to 1.5, and thus the final risk analyses were performed. The risk value shown in these analyses is equal to the average risk of all bridges due to earthquakes. Averaging was used in this section to eliminate independent scenarios. This is so that the final level of risk can be assessed as a parameter independent

of the scenario. Variations in direct, indirect, and total risk are shown in terms of changes in the reconstruction index in Figures 26–30.

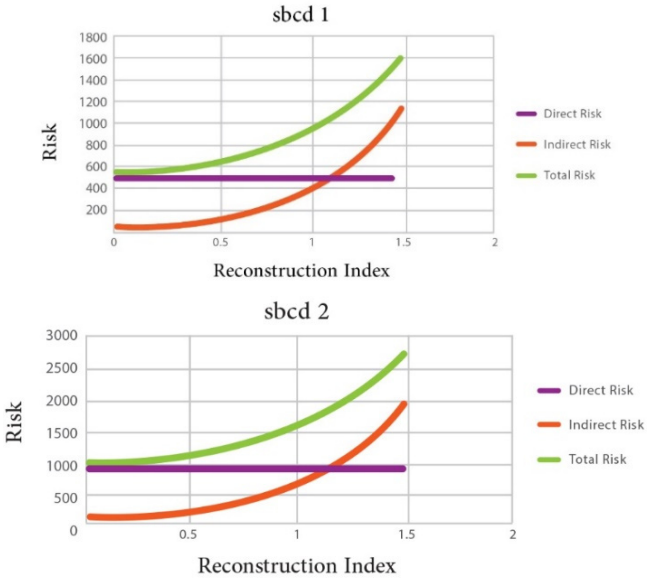

Figure 26. Variations of direct, indirect, and total risk versus changes in the reconstruction index for models sbcd1 and sbcd2.

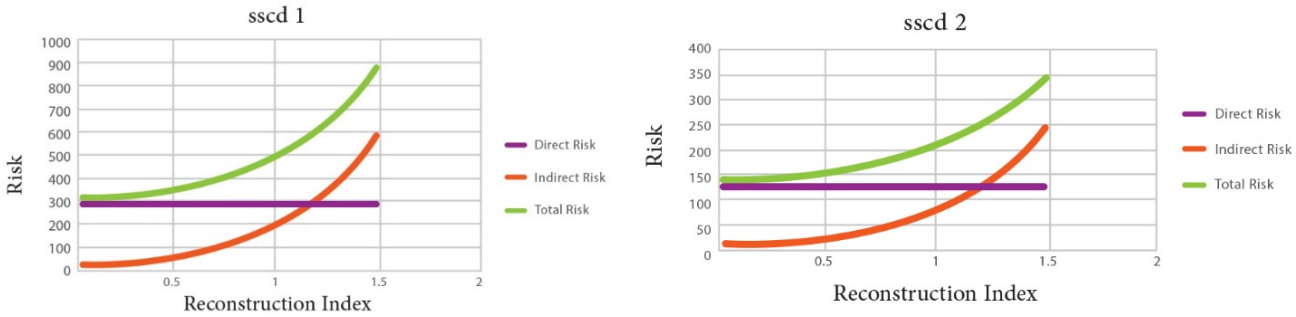

Figure 27. Variations of direct, indirect, and total risk versus changes in the reconstruction index for models sscd1 and sscd2.

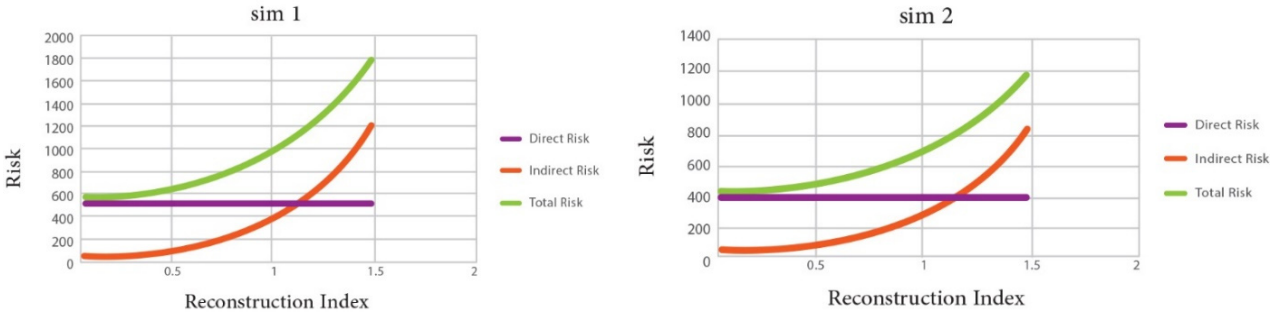

Figure 28. Variations of direct, indirect, and total risk versus changes in the reconstruction index for models sim1 and sim2.

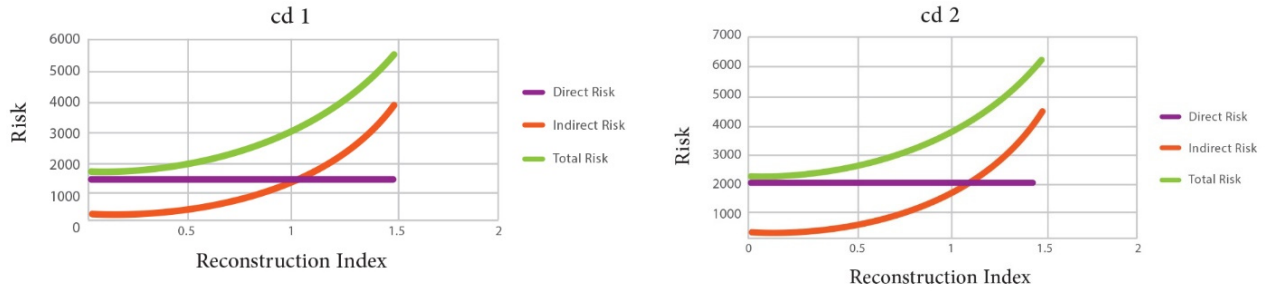

Figure 29. Variations of direct, indirect, and total risk versus changes in the reconstruction index for models cd1 and cd2.

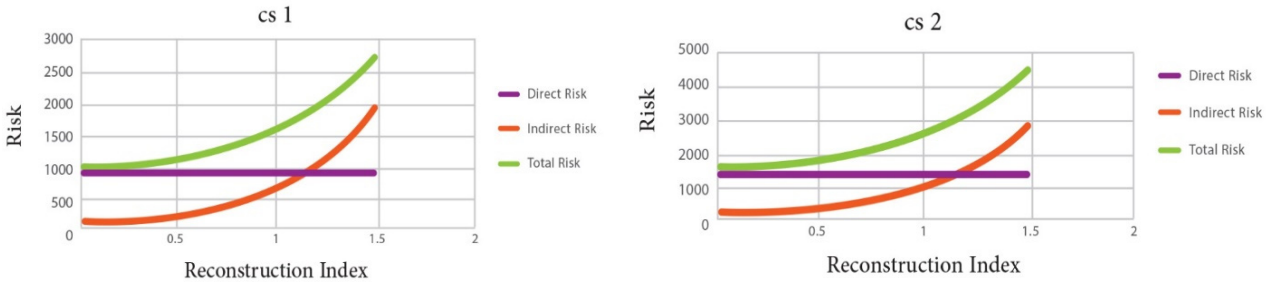

Figure 30. Variations of direct, indirect, and total risk versus changes in the reconstruction index for models cs1 and cs2.

As seen in Figures 26–30, the amount of indirect risk increases exponentially with increases in the reconstruction index (i.e., increasing the time period required for the bridge to return to serviceability). When the reconstruction index is very low, the indirect risk is minor compared to the direct risk caused by the earthquake. However, with increases in the reconstruction index, the relationship grows almost exponentially.

17. Conclusions

This study assessed the probabilistic seismic risks of all highway bridges in Tehran City (the capital of Iran). All 713 highway bridges in Tehran City were divided into six structural systems and according to their age, either less or more than 10 years. Among the 84,000 earthquakes suggested by Zolfaghari's ten-thousand-year catalog, a set of 50 earthquakes was selected via a probabilistic approach via the OPS algorithm to yield the least discrepancy. Based on the fragility curves of different types of bridges available in the literature, weight factors were designated for each of the structural characteristics of bridges, including the materials used, the number of spans and columns, the type of foundation supports, the design codes of each country, the structural system, and the type and method of analysis. Subsequently, decision tree analysis was employed to produce fragility curves for each bridge structural system aged less or more than 10 years. Having the location of each bridge scattered across Tehran City, as well as the software prepared in this research, PGA was calculated at each point of the bridge location using a set of 50 earthquake records. Using the PGA values and the fragility curves, the direct and indirect damage measures imposed on the bridges were estimated. In the end, sensitivity analysis curves for the direct, indirect, and total risks were drawn in terms of the reconstruction index.

The results indicate that, in all cases, the median vulnerability (PGA) decreases by an average of 0.88 with an increase in the bridge age. This means that vulnerability is increased.

According to the results, bridges have the highest degrees of vulnerability in order of simple (highest), steel, concrete slab box, concrete slab–steel box, concrete slab, and steel girder–concrete slab systems. The highest level of vulnerability is related to the bridge with a simple structural system with a median vulnerability of 0.44, and the lowest level

of vulnerability corresponds to the bridge with a steel girder–concrete slab system with a median vulnerability of 0.98, which is about 2.2 times the median vulnerability.

In this research, the results of the sensitivity analysis for direct, indirect, and total risk variations were plotted against changes in the reconstruction index. This was done for each type of structural system. It was revealed that the amount of indirect risk increases exponentially with an increase in the reconstruction index (i.e., increasing the time period required for the bridge to return to serviceability). When the reconstruction index is very low, the indirect risk is small compared to the direct risk caused by the earthquake. However, with increases in the reconstruction index, the relationship rises almost exponentially.

It should be mentioned that the results of this research and the fragility curves presented for each of the structural systems of the bridges were generally calculated using probabilistic methods, which have acceptable accuracy and are very useful for prioritizing bridge strengthening. However, if higher accuracy is needed in case studies, the bridge can be modeled differently.

Author Contributions: Writing—original draft, M.M.; Writing—review & editing, E.P.; Supervision, H.T. All authors have read and agreed to the published version of the manuscript.

Funding: This research was funded by the Babol Noshirvani University of Technology under Grant No. BUT/388011/1402.

Institutional Review Board Statement: Not applicable.

Informed Consent Statement: Not applicable.

Data Availability Statement: Not applicable.

Conflicts of Interest: The authors declare no conflict of interest.

References

1. Naseri, A.; Mirza Goltabar Roshan, A.; Pahlavan, H.; Ghodrati Amiri, G. Effect of curvature radius on probabilistic evaluation of seismic horizontally Curves RC Box girder bridges using Monte Carlo simulation under three-dimensional excitations under Near-Field Earthquakes. *J. Struct. Constr. Eng.* **2021**, *8*, 5–30.
2. Ramanathan, K.N. *Next Generation Seismic Fragility Curves for California Bridges Incorporating the Evolution in Seismic Design Philosophy*; Georgia Institute of Technology: Atlanta, GA, USA, 2012.
3. Mosleh, A. *Seismic Vulnerability Assessment of Existing Concrete Highway Iranian Bridges*; Universidade de Aveiro: Aveiro, Portugal, 2016.
4. Xiang, N.; Alam, M.S. Displacement-Based Seismic Design of Bridge Bents Retrofitted with Various Bracing Devices and Their Seismic Fragility Assessment under near-Fault and Far-Field Ground Motions. *Soil Dyn. Earthq. Eng.* **2019**, *119*, 75–90. [CrossRef]
5. Chen, X.; Li, J.; Guan, Z. Fragility Analysis of Tall Pier Bridges Subjected to Near-Fault Pulse-like Ground Motions. *Struct. Infrastruct. Eng.* **2020**, *16*, 1082–1095. [CrossRef]
6. Naseri, A.; MirzaGoltabar Roshan, A.; Pahlavan, H.; Ghodrati Amiri, G. Numerical Analysis and Vulnerability Assessment of Horizontally Curved Multiframe RC Box-Girder and CFRP Retrofitting of Existing Bridges. *ASCE-ASME J. Risk Uncertain. Eng. Syst. Part A Civ. Eng.* **2022**, *8*, 04022031. [CrossRef]
7. Edwards, P.J.; Bowen, P.A. Risk and Risk Management in Construction: A Review and Future Directions for Research. *Eng. Constr. Archit. Manag.* **1998**, *5*, 339–349. [CrossRef]
8. Birkmann, J. Risk. In *Encyclopedia of Natural Hazards*; Bobrowsky, P.T., Ed.; Encyclopedia of Earth Sciences Series; Springer: Dordrecht, The Netherlands, 2013; pp. 856–862, ISBN 978-1-4020-4399-4.
9. Fedeski, M.; Gwilliam, J. Urban Sustainability in the Presence of Flood and Geological Hazards: The Development of a GIS-Based Vulnerability and Risk Assessment Methodology. *Landsc. Urban Plan.* **2007**, *83*, 50–61. [CrossRef]
10. Tsai, C.-H.; Chen, C.-W. An Earthquake Disaster Management Mechanism Based on Risk Assessment Information for the Tourism Industry-a Case Study from the Island of Taiwan. *Tour. Manag.* **2010**, *31*, 470–481. [CrossRef]
11. Masuya, A. Flood Vulnerability and Risk Assessment with Spatial Multi-Criteria Evaluation. In *Dhaka Megacity: Geospatial Perspectives on Urbanisation, Environment and Health*; Dewan, A., Corner, R., Eds.; Springer Geography; Springer: Dordrecht, The Netherlands, 2014; pp. 177–202, ISBN 978-94-007-6735-5.
12. Li, S.-Q. Comparison of RC girder bridge and building vulnerability considering empirical seismic damage. *Ain Shams Eng. J.* 2023, *in press*. [CrossRef]
13. Zolfaghari, M.R. Development of a Synthetically Generated Earthquake Catalogue towards Assessment of Probabilistic Seismic Hazard for Tehran. *Nat. Hazards* **2015**, *76*, 497–514. [CrossRef]

14. Zare, M.; Bard, P.-Y.; Ghafory-Ashtiany, M. Site Characterizations for the Iranian Strong Motion Network. *Soil Dyn. Earthq. Eng.* **1999**, *18*, 101–123. [CrossRef]
15. Abrahamson, N.A.; Silva, W.J.; Kamai, R. Summary of the ASK14 Ground Motion Relation for Active Crustal Regions. *Earthq. Spectra* **2014**, *30*, 1025–1055. [CrossRef]
16. Boore, D.M. Ground-Motion Prediction Equations: Past, Present, and Future. In Proceedings of the 2014 Annual Meeting of the Seismological Society of America, Anchorage, Alaska, 30 April–2 May 2014; Volume 30.
17. Campbell, K.W.; Bozorgnia, Y. NGA-West2 Ground Motion Model for the Average Horizontal Components of PGA, PGV, and 5% Damped Linear Acceleration Response Spectra. *Earthq. Spectra* **2014**, *30*, 1087–1115. [CrossRef]
18. Chiou, B.S.-J.; Youngs, R.R. Update of the Chiou and Youngs NGA Model for the Average Horizontal Component of Peak Ground Motion and Response Spectra. *Earthq. Spectra* **2014**, *30*, 1117–1153. [CrossRef]
19. Idriss, I.M. An NGA-West2 Empirical Model for Estimating the Horizontal Spectral Values Generated by Shallow Crustal Earthquakes. *Earthq. Spectra* **2014**, *30*, 1155–1177. [CrossRef]
20. Wells, D.; Coppersmith, K. New Empirical Relationships among Magnitude, Rupture Length, Rupture Width, Rupture Area, and Surface Displacement. *Bull. Seismol. Soc. Am.* **1994**, *84*, 974–1002.
21. Bonilla, M.G.; Mark, R.K.; Lienkaemper, J. Statistical Relations Among Earthquake Magnitude, Surface Rupture Length, and Surface Fault Displacement. *Bull. Seismol. Soc. Am.* **1984**, *74*, 2379–2411.
22. Hanks, T.C.; Bakun, W.H. A Bilinear Source-Scaling Model for M-Log a Observations of Continental Earthquakes. *Bull. Seismol. Soc. Am.* **2002**, *92*, 1841–1846. [CrossRef]
23. Avşar, Ö.; Yakut, A.; Caner, A. Analytical Fragility Curves for Ordinary Highway Bridges in Turkey. *Earthq. Spectra* **2011**, *27*, 971–996. [CrossRef]
24. Azevedo, J.; Guerreiro, L.; Bento, R.; Lopes, M.; Proença, J. Seismic Vulnerability of Lifelines in the Greater Lisbon Area. *Bull. Earthq. Eng.* **2010**, *8*, 157–180. [CrossRef]
25. Naseri, A.; Roshan, A.M.G.; Pahlavan, H.; Amiri, G.G. Effects of curvature radius on vulnerability of curved bridges subjected to near and far-field strong ground motions. *Struct. Monit. Maint.* **2020**, *7*, 367.
26. Mander, J.B.; Basöz, N. Seismic Fragility Curve Theory for Highway Bridges. In *Proceedings of the Optimizing Post-Earthquake Lifeline System Reliability*; ASCE: Reston, VA, USA, 1999; pp. 31–40.
27. Choi, E.; Jeon, J.-C. Seismic Fragility of Typical Bridges in Moderate Seismic Zone. *KSCE J. Civ. Eng.* **2003**, *7*, 41–51. [CrossRef]
28. Chang, L.; Elnashai, A.S.; Spencer, B.F., Jr. Post-Earthquake Modelling of Transportation Networks. *Struct. Infrastruct. Eng.* **2012**, *8*, 893–911. [CrossRef]
29. Li, J.; Spencer, B.F., Jr.; Elnashai, A.S. Bayesian Updating of Fragility Functions Using Hybrid Simulation. *J. Struct. Eng.* **2013**, *139*, 1160–1171. [CrossRef]
30. Borzi, B.; Ceresa, P.; Franchin, P.; Noto, F.; Calvi, G.M.; Pinto, P.E. Seismic Vulnerability of the Italian Roadway Bridge Stock. *Earthq. Spectra* **2015**, *31*, 2137–2161. [CrossRef]
31. Karakostas, C.; Makarios, T.; Lekidis, V.; Kappos, A. Evaluation of Vulnerability Curves for Bridges—A Case Study. In Proceedings of the 1st European Conference on Earthquake Engineering and Seismology, Paper, Geneva, Switzerland, 3–8 September 2006.
32. Yamazaki, F.; Motomura, H.; Hamada, T. Damage Assessment of Expressway Networks in Japan Based on Seismic Monitoring. In Proceedings of the 12th World Conference on Earthquake Engineering, Auckland, New Zealand, 30 January–4 February 2000.
33. Karim, K.R.; Yamazaki, F. A Simplified Method of Constructing Fragility Curves for Highway Bridges. *Earthq. Eng. Struct. Dyn.* **2003**, *32*, 1603–1626. [CrossRef]
34. Kibboua, A.; Kehila, F.; Hemaidi-Zourgui, N.; Remki, M. Comparison between Fragility Curves of RC Bridge Piers Designed by Old and Recent Algerian Codes. *Eurasian J. Eng. Sci. Technol.* **2017**, *1*, 56–67.
35. Zourgui, N.H.; Kibboua, A.; Taki, M. Using Full Bridge Model to Develop Analytical Fragility Curves for Typical Concrete Bridge Piers. *Bridges* **2018**, *20*, 519–530. [CrossRef]
36. Lupoi, A.; Franchin, P.; Pinto, P.E.; Monti, G. Seismic Design of Bridges Accounting for Spatial Variability of Ground Motion. *Earthq. Eng. Struct. Dyn.* **2005**, *34*, 327–348. [CrossRef]
37. Moschonas, I.F.; Kappos, A.J.; Panetsos, P.; Papadopoulos, V.; Makarios, T.; Thanopoulos, P. Seismic Fragility Curves for Greek Bridges: Methodology and Case Studies. *Bull. Earthq. Eng.* **2009**, *7*, 439–468. [CrossRef]
38. Nielson, B.G.; DesRoches, R. Analytical Seismic Fragility Curves for Typical Bridges in the Central and Southeastern United States. *Earthq. Spectra* **2007**, *23*, 615–633. [CrossRef]
39. Nielson, B.G. *Analytical Fragility Curves for Highway Bridges in Moderate Seismic Zones*; Georgia Institute of Technology: Atlanta, GA, USA, 2005.
40. Padgett, J.E.; DesRoches, R. Retrofitted Bridge Fragility Analysis for Typical Classes of Multispan Bridges. *Earthq. Spectra* **2009**, *25*, 117–141. [CrossRef]
41. Naseri, A.; Pahlavan, H.; Ghodrati Amiri, G. Probabilistic Seismic Assessment of RC Frame Structures in North of Iran Using Fragility Curves. *J. Struct. Constr. Eng.* **2017**, *4*, 58–78. [CrossRef]
42. Pan, Y.; Agrawal, A.K.; Ghosn, M.; Alampalli, S. Seismic Fragility of Multispan Simply Supported Steel Highway Bridges in New York State. II: Fragility Analysis, Fragility Curves, and Fragility Surfaces. *J. Bridge Eng.* **2010**, *15*, 462–472. [CrossRef]
43. Shinozuka, M.; Feng, M.Q.; Kim, H.-K.; Kim, S.-H. Nonlinear Static Procedure for Fragility Curve Development. *J. Eng. Mech.* **2000**, *126*, 1287–1295. [CrossRef]

44. Banerjee, S.; Shinozuka, M. Nonlinear Static Procedure for Seismic Vulnerability Assessment of Bridges. *Comput.-Aided Civ. Infrastruct. Eng.* **2007**, *22*, 293–305. [CrossRef]
45. Shirazian, S.; Ghayamghamian, M.R.; Nouri, G.R. Developing of Fragility Curve for Two-Span Simply Supported Concrete Bridge in near-Fault Area. *World Acad. Sci. Eng. Technol.* **2011**, *51*, 571–575.
46. Yi, J.-H.; Kim, S.-H.; Kushiyama, S. PDF Interpolation Technique for Seismic Fragility Analysis of Bridges. *Eng. Struct.* **2007**, *29*, 1312–1322. [CrossRef]
47. Rezaei, H.; Zarfam, P.; Golafshani, E.M.; Amiri, G.G. Seismic Fragility Analysis of RC Box-Girder Bridges Based on Symbolic Regression Method. *Structures* **2022**, *38*, 306–322. [CrossRef]
48. Lee, S.M.; Kim, T.J.; Kang, S.L. Development of Fragility Curves for Bridges in Korea. *KSCE J. Civ. Eng.* **2007**, *11*, 165–174. [CrossRef]
49. Zakeri, B.; Ghodrati Amiri, G. Probabilistic Performance Assessment of Retrofitted Skewed Multi Span Continuous Concrete I-Girder Bridges. *J. Earthq. Eng.* **2014**, *18*, 945–963. [CrossRef]
50. Noori, H.Z.; Amiri, G.G.; Nekooei, M.; Zakeri, B. Seismic Fragility Assessment of Skewed MSSS-I Girder Concrete Bridges with Unequal Height Columns. *J. Earthq. Tsunami* **2016**, *10*, 1550013. [CrossRef]
51. Mirza Goltabar Roshan, A.; Naseri, A.; Mahmoodi Pati, Y. Probabilistic Evaluation of Seismic Vulnerability of Multi-Span Bridges in North of Iran. *J. Struct. Constr. Eng.* **2018**, *5*, 36–54. [CrossRef]
52. Pahlavan, H.; Zakeri, B.; Amiri, G.G.; Shaianfar, M. Probabilistic Vulnerability Assessment of Horizontally Curved Multiframe RC Box-Girder Highway Bridges. *J. Perform. Constr. Facil.* **2016**, *30*, 04015038. [CrossRef]
53. Ren, L.; He, S.; Yuan, H.; Zhu, Z. Seismic Fragility Analysis of Bridge System Based on Fuzzy Failure Criteria. *Adv. Civ. Eng.* **2019**, *2019*, 3592972. [CrossRef]
54. Hwang, H.; Jernigan, J.B.; Lin, Y.-W. Evaluation of Seismic Damage to Memphis Bridges and Highway Systems. *J. Bridge Eng.* **2000**, *5*, 322–330. [CrossRef]
55. Naseri, A.; Roshan, A.M.; Pahlavan, H.; Amiri, G.G. Probabilistic seismic assessment of RC box-girder bridges retrofitted with FRP and steel jacketing. *Coupled Syst. Mech.* **2020**, *9*, 359–379.
56. Riga, E.; Fotopoulou, S.; Karatzetzou, A.; Apostolaki, S.; Ntafloukas, K.; Pitilakis, K. Towards the Development of a Seismic Risk Model for Greece. In Proceedings of the International Conference on Natural Hazards and Infrastructure, Chania, Greece, 23–26 June 2019; pp. 16–23.
57. Karimi-Moridani, K.; Zarfam, P.; Ghafory-Ashtiany, M. Seismic Failure Probability of a Curved Bridge Based on Analytical and Neural Network Approaches. *Shock. Vib.* **2017**, *2017*, 2408234. [CrossRef]
58. Esfandiari, Y.; Khorraminejad, A. *Vulnerability Assessment of Multi-Span Simply Supported Concrete Highway Bridges Using Fragility Curves (In Persian)*; Olympic Hotel: Tehran, Iran, 2017.
59. Billah, A.; Alam, M.S.; Bhuiyan, M.R. Fragility Analysis of Retrofitted Multicolumn Bridge Bent Subjected to Near-Fault and Far-Field Ground Motion. *J. Bridge Eng.* **2013**, *18*, 992–1004. [CrossRef]
60. Kaynia, A.M.; Taucer, F.; Hancilar, U. *Guidelines for Deriving Seismic Fragility Functions of Elements at Risk: Buildings, Lifelines, Transportation Networks and Critical Facilities*; Publications Office of the European Union: Luxembourg, 2013; ISBN 978-92-79-28966-8.
61. Jeong, S.-H.; Elnashai, A.S. Probabilistic Fragility Analysis Parameterized by Fundamental Response Quantities. *Eng. Struct.* **2007**, *29*, 1238–1251. [CrossRef]
62. Feng, M.Q.; Shinozuka, M.; Kim, H.-K.; Kim, S.-H. Statistical Analysis of Fragility Curves. *J. Eng. Mech.* **2000**, *126*, 1224–1231. [CrossRef]
63. Saxena, V. *Spatial Variation of Earthquake Ground Motion and Development of Bridge Fragility Curves*; Princeton University: Princeton, NJ, USA, 2000.
64. Balou, M.; Pahlavan, H.; Naseri, A.; Rafiee, F. Seismic Fragility Analysis of Multi-Frame RC Curved Bridges with Base Isolation. *J. Struct. Constr. Eng. Trans. AIJ* **2021**, *8*, 208–224. [CrossRef]
65. Kaveh, A.; Javadi, S.M.; Mahdipour Moghanni, R. Optimization-Based Record Selection Approach to Incremental Dynamic Analysis and Estimation of Fragility Curves. *Sci. Iran.* **2021**, *28*, 700–708.
66. Mogheisi, M.; Tavakoli, H.; Peyghaleh, E. Fragility Curve Development of Highway Bridges Using Probabilistic Evaluation (Case Study: Tehran City). *Asian J. Civ. Eng.* **2023**, *24*, 1783–1800. [CrossRef]
67. Javed, A.; Krishna, C.; Ali, K.; Afzal, M.F.U.D.; Mehrabi, A.; Meguro, K. Micro-Scale Experimental Approach for the Seismic Performance Evaluation of RC Frames with Improper Lap Splices. *Infrastructures* **2023**, *8*, 56. [CrossRef]
68. Shome, N. *Probabilistic Seismic Demand Analysis of Nonlinear Structures*; Stanford University: Stanford, CA, USA, 1999.
69. FEMA. *HAZUS-MH MR1: Technical Manual*; Vol. Earthquake Model; Federal Emergency Management Agency: Washington, DC, USA, 2003.